UNIVERSITAT DE BARCELONA

Bioimpedance & dielectrophoresis instrumentation equipments for living cells manipulation and monitoring

Beatriz del Moral Zamora

ANEX 1–PUBLICATIONS

Authors (signature): del Moral, B; Alvarez-Azpeitia, J.M.; Colomer-Farrarons, J.; Miribel-Catala, P.Ll.; Homs-Corbera, A.; Juarez, A.; Samitier, J.
Title: Towards Point-of-Use Dielectrophoretic Methods: A New Portable Multiphase Generator for Bacteria Concentration
Book: Micro and Nanosystems
Publisher: Bentham Science Publishers Ltd

Towards Point-of-Use Dielectrophoretic Methods: A new Portable Multiphase Generator for Bacteria Concentration

B. del Moral Zamora[1], J.M. Álvarez Azpeitia[2], J. Colomer-Farrarons[1], P.Ll. Miribel-Català[1], A. Homs-Corbera[1,2], A.Juárez[3,4] and J.Samitier[1,2]

1Department of Electronics, Faculty of Physics, University of Barcelona, Martí i Franquès 1, 08028 Barcelona, Spain

2Nanobioengineering group, Institute for Bioengineering of Catalonia (IBEC), Baldiri Reixac 10-12, 08028 Barcelona, Spain

3Microbial biotechnology and host-pathogen interaction group, Institute for Bioengineering of Catalonia (IBEC), Baldiri Reixac 10-12, 08028 Barcelona, Spain

4 Department of Microbiology, Faculty of Biology, University of Barcelona, Diagonal 643, 08028 Barcelona, Spain

Abstract—**This manuscript presents a portable and low cost electronic system for specific point-of-use dielectrophoresis applications. The system is composed by two main modules: a) a multiphase generator based on a Class E amplifier, which provides 4 sinusoidal signals (0º, 90º, 180º, 270º) at 1 MHz with variable output voltage up to 10 Vpp (Vm) and an output driving current of 1 A; and b) a dielectrophoresis-based microfluidic chip containing two interdigitated electrodes. The system has been validated by concentrating *Escherichia Coli* (*E. Coli*) at 1 MHz while applying a continuous flow of 5 µL/min. The device functionalities were verified under different conditions, achieving an 83% trapping efficiency when counter-phased signals are used.**

Keywords— **Dielectrophoresis, Cell Concentrator, electronics, lab-on-a-chip (LOC), portable device, low cost, Class E amplifier**

I. Introduction

Since Pohl [1] discovered the dielectrophoretic effect (DEP) there has been an increase of interest in using this particle manipulation technique, especially in the last decade [2]. The evidence is the large number of scientific publications that appear each year regarding the different applications of DEP: concentrate [3], sort [4], rotate [5] and move [6-7] particles or biological material. In fact, all these works are the consequence of DEP versatility since it can be used in several applications, such as microfluidics [8], medical diagnostics [9] or biosensors [3, 10-11]. Thus, DEP has the potential of revolutionizing the medical community and in fact, new ways to further investigate unknown diseases are being opened. An example of this medical advances are studies such as the one by *N.Swami et al* [10] which has achieved enhancement of DNA hybridization kinetics through DEP and has improved the detection limit of their sensors by 10-fold, or the results presented by [9] *H.Shafiee et al*, where they have demonstrated the potential of contactless DEP to separate and individuate rare cells.

Nowadays, these DEP applications are requiring new DEP system functionalities. Thus, new electronic devices for DEP experiences were being developed to meet these demands [13-16, 6]. For example in [16], the presented tumor cells concentrator is achieved through a microfluidic chip with curvy arrays and an electronic circuit that generates stepping electric fields. However, it is still difficult to find tailor-made electronic devices for DEP applications, combining microfluidics and electronics for a portable DEP system. Usually, regular multiple-use commercial devices have a high cost and large dimensions, which is a disadvantage in many applications.

We present a portable and low cost system (Fig. 1) for DEP applications. The system is composed of a microfluidic chip, comprising two interdigitated electrodes, and an electronic multiphase generator specifically designed for DEP applications. The generator allows DEP electric field control by combination of four driving available phases φ1=0º, φ2=90º, φ3=180º and φ4=270º) or by varying the amplitude of each one of these driving signals (Vm) up to 10 Vpp.

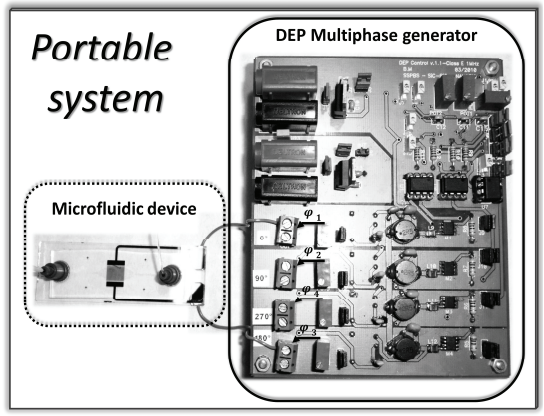

Fig 1. Portable and Low cost designed system, composed of the multiphase Generator and a microfluidic device.

The system has been tested using bacteria concentration experiments at continuous flow rate. This application is needed for many biomedical, food-control or environmental

analysis situations, where bacteria or cells are recuperated from large volumes of sample and need to be concentrated [3, 10-11] before being analyzed. In our case, *E. Coli* has been concentrated. This bacterium is a member of the family *Enterobacteriaceae* [17] which is located in the intestine of humans and warm-blooded animals [18]. Some *E. Coli* strains are pathogenic for the humans and produce infections or gastrointestinal diseases [19]. That occurs when bacteria is transmitted through water or food [18-20] by fecal contamination, due to unsanitary conditions. Its presence is commonly analyzed with a coliform detection by lactose fermentation [20-21]. However, this method is a lengthy process [21] that could be improved using DEP-based concentration devices. Our designed portable system provides a method to concentrate bacteria and we have proved its usefulness on *E. Coli* samples while applying their optimal trapping frequency (1 MHz), as it will be explained later on. Experiments have been done at different applied voltages and different phase combinations, maintaining the same DEP effect between the different analyzed cases, so as to check the available options of the DEP multiphase generator.

II. Theory

The dielectrophoresis [1] is the movement of an electrically neutral particle when a non-uniform electric field is applied. This effect is defined in terms of DEP force. If it is considered a homogeneous isotropic particle which is polarized linearly, the force is defined by (1) [22-23].

$$F_{DEP} = \frac{1}{2} V \bullet Re[\alpha^*(\omega)] \nabla |E|^2 \quad (1)$$

Where E is the electric field, V is the volume of the particle and α is the effective polarizability, which is defined as follows (2).

$$\alpha = 3\varepsilon_0 \varepsilon_m F_{CM} \quad (2)$$

ε_0 and ε_m are the vacuum permittivity and the medium permittivity respectively, and F_{CM} is the Clausius-Mosotti Factor. According to the expressions (1-2), α sign, and the electric field gradient, describe the force direction. When a positive α factor is obtained, the particle is attracted to an electric field maximum or to a region with high electric field intensity (which is called positive DEP or p-DEP). Otherwise, the particle is attracted to an electric field minimum (negative DEP or n-DEP). Hence, DEP allows controlling the movement of a particle by modifying the electrical properties of the medium. Moreover, the DEP effect can also be modified by varying the applied signal in terms of phase (φ), frequency (ω) and voltage level (Vm). Furthermore, changing the electrode shape, or alternatively placing dielectric structures strategically, also create different DEP forces by affecting the electric field uniformity. In this study, DEP force is modified using different phase combinations and by varying the applied voltage.

Our microfluidic device was tested by concentrating *E. coli* cells. In order to define a suitable trapping frequency, the DEP expressions should be adapted to the *E. coli* dielectric model. If this bacterium is considered as an ellipsoid shape with two dielectric layers [24], the adapted Clausius – Mosotti factor is as follows:

$$F_{CM_i}(\omega) = 1/2 \cdot \left(\varepsilon_p^* - \varepsilon_m^* / \varepsilon_m^* + A_i\left(\varepsilon_p^* - \varepsilon_m^*\right)\right) \quad (3)$$

where ε_p is the particle permittivity and Ai is the depolarization factor of an individual ellipsoid axe (i =*x,y,z*), which for the large axis is

$$A_x = (1 - e^2)/(2e^3) \log(1 + e/((1 - e) - 2e)) \quad (4)$$

where e is the eccentricity that involves the ellipsoid dimensions (b being the height and a the width),

$$e = \sqrt{(1 - (b/a)^2)} \quad (5)$$

Moreover, the depolarization factor for the shorter axis is

$$A_z = A_y = (1 - A_x)/2 \quad (6)$$

Thus, the expression (3) represented in [25], indicates that the theoretical range to manipulate *E. Coli* by means of p-DEP is 500 kHz-10 MHz, with the sample conductivity used in our work, discussed in section III.B. Also, the maximum *E. Coli* p-DEP trapping force for our given media conductivity was obtained around 1 MHz, which is the working frequency value of the designed generator.

III. Materials and Methods

A. Bacterial strains and culture media

E. Coli 5K cells were grown overnight in 10 mL Luria–Bertani broth at 37 °C. The obtained cell concentration (estimated by performing viable counts in LB agar) was 10^9 bacteria/mL. *E. Coli* experimental samples for DEP were obtained by first pelleting an overnight culture using centrifugation at 5000 rpm for 5 minutes and re-suspending the cells in 10 mL deionized water. Then they were diluted to achieve a final cell concentration around $2.4 \cdot 10^3$ bacteria/μL. The conductivity of the experimental *E. Coli* samples was 11.38 μS/cm, measured by a conductivity meter (Corning™ 441). After that, samples at this final concentra-

tion were separated and frozen in different 1 mL collecting tubes for further experimental use.

B. Numerical modelling

The DEP force inside the used microfluidic device was simulated by a Comsol© Multiphysics 4.2a electrostatic module. This allowed predicting the behaviour of the chip in dielectrophoretic terms. A small differential of the microfluidic chip chamber (350 µm x 200 µm x 50 µm), with gold electrodes separated 50 µm between them, was designed with Solidworks CAD programme. Then file was exported to Comsol and symmetry boundary conditions were applied so as to emulate the full microfluidic chamber.
To introduce the electric field in the medium, the electrodes from the model were activated by two signals, considering two cases:
A) The single phase case (see Case 1 in Results), which represents the standard signal distribution for DEP concentration. In here, a signal of 10/√2VRMS was set in Electrode 1 and Electrode 2 was connected to reference (0 V) during the simulation.
B) The counter-phased case (see Case 5 in Results), which doubles the effective voltage inside the microfluidic chamber. In this case, simulation was run after setting the electric potential conditions on the two electrodes to 10/√2VRMS and -10/√2VRMS respectively. This simulated the counter-phased signals effect r.
After, *E. Coli* parameters related to DEP expression were introduced as global definitions. Hereinafter, and a stationary analysis was performed and the DEP expression was represented in a slice of the chamber.The obtained results are shown in Fig. 2, where Fig.2.A represents the defined single phase case for a lateral view of the chamber. Moreover, in Fig.2.B the results of using counter-phased signals are also showed. As it can be observed, applying always the same voltage signal, different relative forces values were obtained only by changing the phase configuration. Thus, the simulation results suggested that better efficiencies will be obtained for the counter-phased signals case, since higher DEP attraction is expected. Furthermore, obtained red areas (the higher DEP force zones) suggested that *E.Coli* trapping will take place in the edges of the electrodes and not much further up from electrode, as already well-known in literature. Thus, with this type of electrode-chamber combinations, a large chamber with many interdigitated structures is needed so as to increase the trapping area and consequently increase the bacterium capture efficiency.

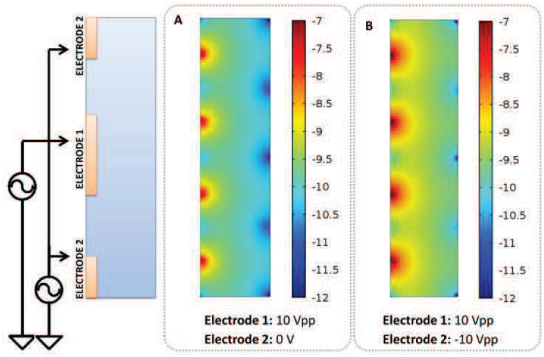

Fig. 2. DEP force (log (N)) distribution simulation. On the left of the picture a scheme of signal injection and electrode distribution is represented. A. Single fase (Case 1 of the study). B. Counter-phased signals (Case 5 of the study)

C. Microfluidic device fabrication process

The microfluidic chip fabrication (Fig. 3) can be divided into three main steps: microchannel molding, electrode fabrication and microfluidic chip bonding. Each process will be detailed as follows.

The first process is the SU8 50 (MicroChem™) master fabrication over glass slides (Deltalab™). It begins with a slide cleaning and an activation protocol based on Piranha attack during 15 minutes. Then, a 50 µm high SU-8 50 (MicroChem™) is spun over glass slides. Once developed, the desired microchannel mold is obtained. To replicate this microchannel, a 10:1 ratio PDMS pre-polymeric solution (Dow Corning™ Sylgard®184) has to be mixed, degased and poured into the mold. Later, after a 70ºC at 1h curing process, the casted PDMS is peeled off from the master.

In order to fabricate the microelectrodes a lift-off soft lithography process is applied. First, the same initial Piranha chemical attack is used over the glass slide. The AZ 1512 (AZ Electronic Materials™) photoresist was chosen to act as a sacrificial layer. After an exposure and a first development of the AZ 1512, two metal layers, formed by 20 nm of Ti and 80 nm of gold, are vapor-deposited onto the surface. The final design of the electrodes is obtained by removing the remaining sacrificial layer of AZ photoresist with the AZ 726 MIF developer.

Once the PDMS replica and the microelectrodes are finished, the microfluidic chip has to be sealed. The first step is surface cleaning using an oxygen plasma process (PDC-002, Harrick Scientific Corporation. Ithaca) for 15 minutes.

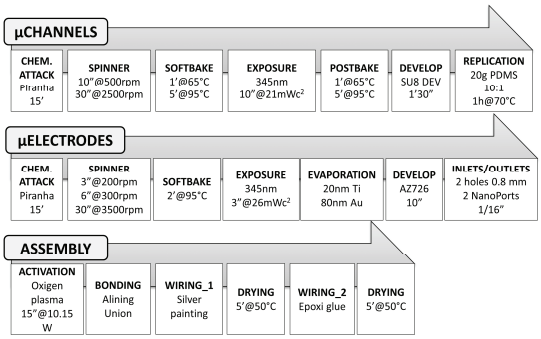

Fig. 3. Microfluidic device fabrication. Scheme of the fabrication process and its steps.

The PDMS channels are finally aligned and attached by contact to the glass substrate to form an irreversible bond. The complete microfluidic chip is finished by connecting one cable to each pad. The welding between cable and pad is achieved by applying conductive silver paint (RS 186-3593, RS Components), which acts as connective soldering glue. The soldered parts are then dried at room temperature for 30 minutes. Once dried, an epoxy glue mix is also applied and cured at room temperature for a further 60 minutes to increase the mechanical properties of the cold-soldered union. Finally, two Nanoport Assemblies (Upchurt Scientific™) are attached, in order to set the inlet and outlet connections of the microfluidic chip by means of 1/32'of inner diameter tube.

D. DEP multiphase generator

A full custom electronic circuit was specifically designed to dielectrophoretic *E. coli* manipulation by means of the designed microfluidic chip.

Dielectrophoresis allows controlling the movement of a particle in a liquid varying the electric field non-uniformity (by changing electrodes shape or disposition, or by placing dielectric structures strategically), but also its frequency, its power, and the medium electrical properties [24]. Furthermore, it is possible to take advantage of the applied signal phase to produce higher electric fields inside the microfluidic chip, and also to avoid possible DC-offsets due to mismatches. Moreover, the use of multiple phases allows performing other DEP-based manipulation effects such as particle rotations or travelling-wave dielectrophoresis [4,6, 25-26].

Thus, the DEP multiphase generator and its specifications were defined taking into account: a) the *E. coli* behavior [24] in terms of dielectrophoretic force or Clausius-Mossotti factor (considering the sample conductivity was 11.38 µS/cm), as it was defined in II. For this reason, in order to obtain the maximum positive DEP force, the operation frequency was set to 1MHz [25]. b) Considering future new ways of bacteria manipulation by means of multiphase signals. Thus, 4 different channels with different phases were-defined to provide multiple *E.coli* manipulation options. Thereby, by taking advantage of diphased signals, it will be possible to apply higher effective voltages inside the microfluidic chip, such as the use of counter-phase signals. Thus, when two counter-phase signals (with the same ground reference) are applied to the electrodes, the effective applied voltage to the chip (V_T) is defined by the following equation:

$$V_T = \left[{V_m}^{\varphi 1}\sin(\omega t) + V_{01}\right] - \left[-{V_m}^{\varphi 2}\sin(\omega t) + V_{02}\right] \quad (7)$$

where ${V_m}^{\varphi X}$ is the amplitude peak voltage of the signal, and V_{01} and V_{02} are the offset voltages. However, if the two peak amplitudes voltages are considered equals,

$${V_m}^{\varphi 1} = {V_m}^{\varphi 2} = V_m \quad (8)$$

the resultant effective applied voltage signal is

$$V_T = 2[V_m \sin(\omega t)] + (V_{01} - V_{02}) \quad (9)$$

By the analysis of expression (9) it is conclude that the effective voltage V_T is doubled. This effect will allow injecting higher voltages inside the microfluidic chip, so as to increase the electric field intensity. Consequently it could be possible to increase DEP force. Furthermore, expression (9) indicates the average offset of the resultant applied signal ($V_0 = V_{01} - V_{02}$) could be reduced near zero and considered null. This also increase interest on using this configuration, since offset voltage (V_0) could cause electrolysis and fast degradation on the electrode [27-28] if no isolating area is used.

Hence, the final electronic architecture used is presented in Fig. 4. It is mainly formed by three modules (Fig. 4): a) A low power signal generator which creates four shifted and frequency stable signals to control the output module. b) A driver which adapts the signal to the desired level of current for the next stage. c) A class E amplifier which creates the DEP signals. The first module (a), the low power signal generator, is based on the LTC6902 (Linear Technology), which generates four squared signals (Fig. 4. d) synchronized between them and whose outputs are shifted φ1, φ2, φ3 and φ4 respectively. The LTC6902 output frequency operation is selected according to the expression (10):

$$f_{out} = (10\,MHz\,(20k\Omega/R\_set\,))/(N \cdot M) \quad (10)$$

Where *R_set* is the frequency selector resistance (see Fig. 4, a) which is set according to the desired output frequency, *M* is the number of phases that were used, actually 4, and *N* defines the working frequency range (according to

LTC6902 datasheet *N*=10 to work between 200 kHz and 2 MHz).

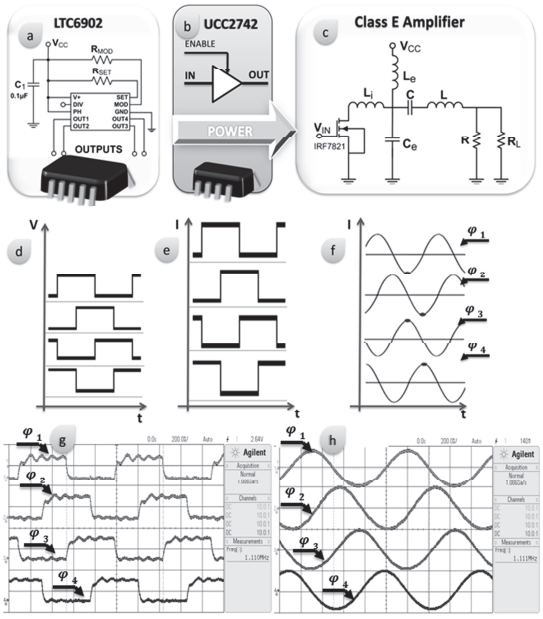

Fig. 4. DEP generator bloc diagram and related signals. The DEP generator is mainly composed of three modules: The LTC6902 square generator (a), the UCC2742 power driver (b) and the designed Class E Amplifier (c). Their respective output signals are shown at the bottom, where (d) is related with (a), (e) with (b) and (f) with (c). Moreover, experimental signals from DEP Multiphase Generator are shown in (g) and (h). The UCC2742 output signal is shown on the (g). On (h) a capture from the four outputs is depicted.

This chip is prepared for low voltage designs since it only supplies 400 µA. Following our purpose, a Driver UCC27424 (Texas Instruments) is used (module b), which increases the current levels of the signals (up to 4 A) as it is depicted in Fig. 4. e.

Then, the driving signals control the final module (c) which is composed of a sinusoidal generator circuit which is based on a Class E amplifier. This structure (Fig. 4.c circuit) is capable of generating high frequency signals with a stable output voltage [29-30]. This amplifier configuration presents a high output current capability. Thus, it has the capacity to drive large arrays of electrodes or interdigitated structures. The circuit is composed of an inductor L_e working as a current source, a capacitor C_e and a resonant tank, composed of an inductor *L* and a capacitor C, which resonate at the selected frequency. Thus, the amplifier creates a sinusoidal signal (Fig. 4.f) which follows the frequency of the driving signal created in the previous modules and introduced by a power transistor NMOS. The Class E parameters (*Le, Ce, C, L, R*) could be tuned using the following expressions (11-14). Note that *RL* is the equivalent resistance of the microfluidic chip and the inductive element *Li* is introduced to reduce the instant power demand of the system, due to the commutation from the square signal input, in Fig.4.c

$$L_e = \frac{0{,}4001R}{\omega_s} \tag{11}$$

$$C_e = \frac{2{,}165}{R\omega_s} \tag{12}$$

$$L = \frac{QR}{\omega_s} \tag{13}$$

$$\omega_s L = \frac{1}{C\omega_s} = 0{,}3533 \tag{14}$$

Thus, four independent channels perfectly synchronized at *φ1, φ2, φ3* and *φ4* are obtained. The generator outputs are selectable and allow varying output voltage up to 10 Vpp.
Additionally, the output signals of the DEP multiphase generator are depicted in Fig. 4.h (real caption obtained by Agilent DSO-X-2014 Oscilloscope), where the four channels are operating at 10 Vpp at the same time and the diphase between waves and their frequency can be observed. Also it is shown how the outputs follow the frequency and the diphase (related to 0º signal) of the driving signal (Fig. 4.g), which controls the Class E Amplifier activation and was generated in first module (Fig. 4.a).
Finally, from the test of the designed board, the general features of the device are obtained and showed on Table 1, where it is remarkable the variable output range of the device, the generated phased versatility and the current capability of the circuit, which gives rise to future applications with other electrode disposition or the use of other medias with higher conductivities.

Table 1 DEP multiphase generator. General features

Vsupply 1	*5 V_{DC}*
Vsupply 2	1-15 V_{DC}
Available channels	4
Output phases	0º, 90º, 180º, 270º
Working frequency	1 MHz
Vout range (peak voltage)	1 V- 10 V
Total output current capability	1 A

E. Experimental Setup

The experimental setup defined for each experiment of this study is shown in Fig. 5. The complete microfluidic module is composed of a 6 port manual valve (Valco), con-

nected to a 5 mL syringe mounted in an infusion micropump (Cetoni NEMESYS). The valve is connected to the microfluidic chip, through the nanoports (Upchurt Scientific™), by means of FEP tube of 1/32' of inner diameter from IDEX™. This was placed over an inverted microscope stage (Olympus IX71) with a digital camera (Hamamatsu Orca R2) so as to verify the effects of the dielectrophoresis inside the microfluidic chip. Moreover, the microfluidic chip electrodes were activated by the DEP multiphase generator defined in previous sections. Finally, a power source (Agilent E3631A) was used to power it in this case, so as to check board during the experimental.

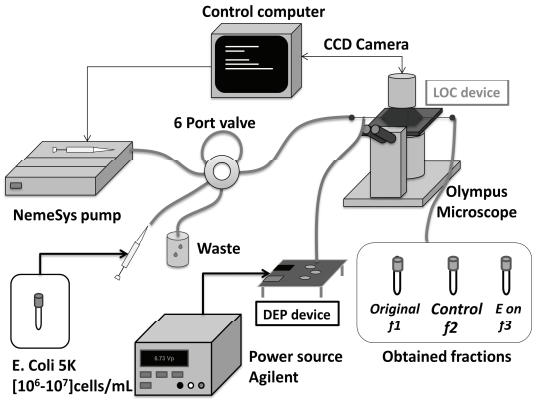

Fig.5. Experimental Setup

F. Experimental Protocol

In order to analyze the device trapping efficiency, three fractions of bacteria were obtained from each experimental process (Fig. 5): the original fraction (*f1*), the control fraction (*f2*), and the field action escaped bacteria's fraction (*f3*). The fractions f2 and f3 were obtained after introducing 150 µL of *E. Coli* sample (50 µL of original sample diluted in 100 µL of deionized water during the experimental process). Hence, in this particular case, a maximum concentration factor of 3 is possible, since the sample is concentrated in a volume of 50 µL.

The next protocol was followed in order to obtain every fraction: a 1 mL tube was defrosted to collect the first 50 µL sample (*f1*).The 1 mL tube's remaining content was introduced into the microfluidic module by 50 µL loads through the valve. After the first load injection without electric field activation, the second fraction (*f2*) was collected. Then, after a second load injection and keeping the electric field activated, a third fraction (*f3*) was collected. Every fraction was obtained at a constant 5 µL/min flow rate by continuous deionized water pumping. Moreover, each 150 µL fraction was diluted again until reaching 200 µL, owing to the cytometer specifications, and immediately frozen to -20 °C so as to ensure that all the collected samples are in the same conditions before being analyzed. Once the fractions were defrosted, a flow cytometry (Beckman Coulter FC 500) bacteria counting process was applied. Moreover, in order to improve the analysis accuracy, 1 µL of Green Fluorescent Nucleic Acid Stain (Invitrogen SYTO 13) was added to each 200 µL fraction.

IV. Results

In order to verify the system functionality, five series of concentration experiments were planned. These are defined in Table 2.

Table 1 Experimental Cases

Experimental Case	Applied signals	Resultant potential V_{RMS}	Applied voltage $V_{pp} = 2V_m$	Case 1 Equivalent voltage
Case 1- Single Phase **(reference)**	E1: φ_1= 0º E 2: GND	$V_m/\sqrt{2}$	10Vpp	--
Case 2 90ºdiphase	E1: φ_1= 0º E2: φ_2= 90	V_m	7Vpp	10Vpp
Case 3 270ºdiphase	E1: φ_1= 0º E2: φ_4= 270º	V_m	7Vpp	10Vpp
Case 4 180ºdiphase	E1: φ_1= 0º E2: φ_3= 180º	$\sqrt{2}V_m$	5Vpp	10Vpp
Case 5 180ºdiphase	E1: φ_1= 0º E2: φ_3= 180º	$\sqrt{2}V_m$	10Vpp	20Vpp

Vm=maximum applied voltage. E1, E2= electrode 1 and 2.

The functionality of all DEP multiphase generator channels was tested with four different experiments. Two signals from the device channels were applied to the pair of interdigitated electrodes, creating different phase combinations which generate the same DEP effect. Each applied voltage was determined by equalizing the resultant potential of each pair of applied signals (V_{RMS}) to Case 1 (see Table 2). Hence, cases 1, 2, 3 and 4, it was expected to obtain similar concentration efficiencies since all of them had equivalent applied fields. Supplementary to these, Case 5 was defined to verify if counter-phase signals could be the best option for concentration purposes, since it was expected to obtain better results with the same Vm per channel (maximum voltage) applied as in Case 1 and with the double voltage as compared with Case 4. This case corresponds to simulation B from Numerical Modeling section (Fig. 2.B).

Thus, six repetitions of each Case were done to obtain statistics of concentration efficiency. Thus, the sample extraction protocol described in section III.F was followed. Then, from each individual experiment a cytometric result

was obtained. From this exhaustive cell counts, the trapping efficiency for each experiment was calculated, by means of the following expression (15)

$$Trapping\ (\%) = \frac{f2-f3}{f2} \bullet 100 \qquad (15)$$

Experimental results are depicted on Fig. 6. The median and the quartiles of each sample group (Cases) are presented in order to give a visual representation of the sample group distribution. As it was expected, similar efficiencies were obtained for equivalent cases (Cases 1, 2, 3 and 4), since all of them have the same applied effective voltage. Nevertheless, for Case 5, a higher efficiency was observed, which confirmed the results obtained in the previous simulations. In fact, a median efficiency of 83% was obtained, while the previous cases shown an average 75%. In addition, counter-phased cases (Case 4 and Case 5) were observed to have less dispersion, comparing to the rest of cases. Furthermore, in this case DC offset effect was reduced.

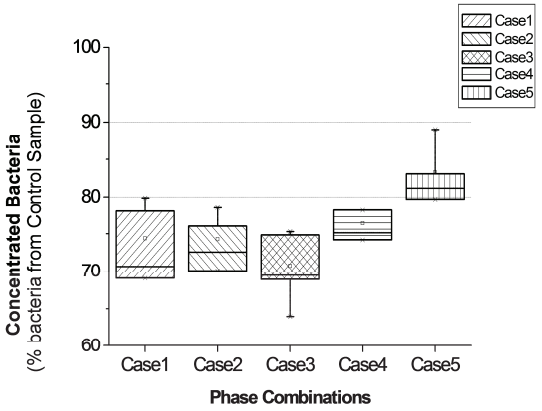

Fig. 6. Percentage of trapped bacteria for the different experimental presented cases.

Additionally, so as to report a statistical analysis, the obtained bacteria counts were introduced in SPSS Statistics Software (IBM). Since the obtained counts are independent samples, a non-parametrical test was done in order to analyze the obtained results. Thus a U-Mann Whitney test was carried out, where equivalent effective-voltage Cases (Case 1, 2, 3 and 4) were analyzed in pairs. Then, no significant differences were obtained for these Cases. Moreover, these Cases were compared with the double voltage Case (Case 5). In this test significant differences between samples were detected, since Case 5 presents a higher trapping efficiency due to its equivalent applied voltage of 20 Vpp. Hence, the results conclude that the use of counter-phased signals are the best option for a properly *E.Coli* trapping which allows the use of the same instrument to increase efficiency while reducing the risks of DC components leading to electrolysis.

V. CONCLUSIONS

A multiphase generator, which is first approach of a final envisaged portable system, has been designed for easiest concentration analysis setup. This is actually working at the optimal *E. Coli* p-DEP trapping frequency of 1 MHz. The DEP generator presents a variable output voltage range and a current capability up to 1A. Thus, new trends are created for the use of the device become possible, such as more conductive mediums or other electrode structures.

The device has been tested and validated in a series of *E. Coli* concentration experiments with exhaustive cellular counts. The experiments were done at different phase combinations with equivalent DEP effects and with 150 µL of diluted E. Coli samples and an average concentration of $2.4 \cdot 10^3$ bacteria/ µL, at 5 µL/min continuous flow rate. From the analysis of these experiments, a concentration efficiency of 75% was obtained. However the concentration would further increase for larger initial samples due to the continuous flow configuration. Consequently, more bacteria would be trapped in the same volume although this would be at the expense of longer concentration times.

Furthermore, it has verified the benefits of the equipment for counter-phased uses. In this method, an 83% trapping efficiency was obtained when the applied voltage was doubled. Moreover, the electrode degradation due to electric DC offset was reduced in this case.

ACKNOWDLEGMENTS

We would like to express our gratitude to Mª Carmen Jaramillo for the offered support in the bacteria treatment.

CIBER-BBN is an initiative funded by the VI National R&D&i Plan 2008-2011, Iniciativa Ingenio 2010, Consolider Program, CIBER Actions and financed by the Instituto de Salud Carlos III with assistance from the European Regional Development Fund.

The Nanobioengineering group has support from the Commission for Universities and Research of the Department of Innovation, Universities, and Enterprise of the Generalitat de Catalunya (2009 SGR 505).

This material is based upon work supported by the Botin Foundation, Santander, Spain.

References

[1] Pohl, H. A.; Hawk, I. Separation of Living and Dead Cells by Dielectrophoresis. *Science.* **1966**, *152*, 647.

[2] Pethig, R. Review Article—Dielectrophoresis: Status of the Theory, Technology, and Applications. *Biomicrofluidics* **2010**, *4*, 22811.

[3] Hamada, R.; Takayama, H.; Shonishi, Y.; Hisajima, T.; Mao, L.; Nakano, M.; Suehiro, J. Improvement of Dielectrophoretic Impedance Measurement Method by Bacterial Concentration Utilizing Negative Dielectrophoresis. In *Journal of Physics: Conference Series*; IOP Publishing, 2011; Vol. 307, p. 12031.

[4] Van den Driesche, S.; Rao, V.; Puchberger-Enengl, D.; Witarski, W.; Vellekoop, M. J. Continuous Cell from Cell Separation by Traveling Wave Dielectrophoresis. *Sensors Actuators B Chem.* **2011**.

[5] Ino, K.; Ishida, A.; Inoue, K. Y.; Suzuki, M.; Koide, M.; Yasukawa, T.; Shiku, H.; Matsue, T. Electrorotation Chip Consisting of Three-Dimensional Interdigitated Array Electrodes. *Sensors Actuators B Chem.* **2011**, *153*, 468–473.

[6] Issadore, D.; Franke, T.; Brown, K. A.; Westervelt, R. M. A Microfluidic Microprocessor: Controlling Biomimetic Containers and Cells Using Hybrid Integrated Circuit/microfluidic Chips. *Lab Chip* **2010**, *10*, 2937–2943.

[7] Cheng, I. F.; Chung, C. C.; Chang, H. C. High-Throughput Electrokinetic Bioparticle Focusing Based on a Travelling-Wave Dielectrophoretic Field. *Microfluid. Nanofluidics* **2011**, *10*, 649–660.

[8] Wang, Y.; Ye, Z.; Ying, Y. New Trends in Impedimetric Biosensors for the Detection of Foodborne Pathogenic Bacteria. *Sensors (Basel).* **2012**, *12*, 3449–71.

[9] Shafiee, H.; Caldwell, J. L.; Sano, M. B.; Davalos, R. V. Contactless Dielectrophoresis: a New Technique for Cell Manipulation. *Biomed. Microdevices* **2009**, *11*, 997–1006.

[10] Shafiee, H.; Sano, M. B.; Henslee, E. A.; Caldwell, J. L.; Davalos, R. V. Selective Isolation of Live/dead Cells Using Contactless Dielectrophoresis (cDEP). *Lab Chip* **2010**, *10*, 438–445.

[11] Swami, N.; Chou, C. F.; Ramamurthy, V.; Chaurey, V. Enhancing DNA Hybridization Kinetics through Constriction-Based Dielectrophoresis. *Lab Chip* **2009**, *9*, 3212–3220.

[12] Puttaswamy, S. V; Su, Y. J.; Sivashankar, S.; Yang, S. M.; Yang, Y. S.; Liu, C. H. Dielectrophoretic Concentrator for Enhanced Performance of Poly-Silicon Nanowire Field Effect Transistor for Biosensing Application. In *Micro Electro Mechanical Systems (MEMS), 2012 IEEE 25th International Conference on*; IEEE, 2012; pp. 1305–1308.

[13] Baylon-Cardiel, J. L.; Jesús-Pérez, N. M.; Chávez-Santoscoy, A. V; Lapizco-Encinas, B. H. Controlled Microparticle Manipulation Employing Low Frequency Alternating Electric Fields in an Array of Insulators. *Lab Chip* **2010**, *10*, 3235–3242.

[14] Hunt, T. P.; Issadore, D.; Westervelt, R. M. Integrated Circuit/microfluidic Chip to Programmably Trap and Move Cells and Droplets with Dielectrophoresis. *Lab Chip* **2007**, *8*, 81–87.

[15] Miled, M. A.; Sawan, M. A New Fully Integrated CMOS Interface for a Dielectrophoretic Lab-on-a-Chip Device. In *Circuits and Systems (ISCAS), 2011 IEEE International Symposium on*; IEEE, 2011; pp. 2349–2352.

[16] Qiao, W.; Cho, G.; Lo, Y. H. Wirelessly Powered Microfluidic Dielectrophoresis Devices Using Printable RF Circuits. *Lab Chip* **2011**, *11*, 1074–1080.

[17] Jen, C.-P.; Huang, C.-T.; Chang, H.-H. A Cellular Preconcentrator Utilizing Dielectrophoresis Generated by Curvy Electrodes in Stepping Electric Fields. *Microelectron. Eng.* **2011**, *88*, 1764–1767.

[18] Ewing, W. H. *Edwards and Ewing's Identification of Enterobacteriaceae*; Elsevier Science Publishing Co. Inc., 1986.

[19] Gibson, G. R.; Macfarlane, G. T.; others. *Human Colonic Bacteria: Role in Nutrition, Physiology, and Pathology.*; CRC Press Inc., 1995.

[20] Feng, P. Escherichia Coli Serotype O157: H7: Novel Vehicles of Infection and Emergence of Phenotypic Variants. *Emerg. Infect. Dis.* **1995**, *1*, 47.

[21] Feldsine, P. T.; Falbo-Nelson, M. T.; Hustead, D. L. ColiComplete® Substrate-Supporting Disc Method for Confirmed Detection of Total Coliforms and Escherichia Coli in All Foods: Comparative Study. *J. AOAC Int.* **1994**, *77*, 58–63.

[22] Pouch Downes, F.; Ito, K. *Compendium of Methods for the Microbiological Examination of Foods*; 4th ed.; American Public Health Association, 2001; p. 676.

[23] Morales, F. H. F.; Duarte, J. E.; Martí, J. S. Modelado y simulación de microestructuras para la manipulación de micropartículas. *Rev. la Acad. Colomb. ciencias exactes, fisicas y Nat.* **1936**, *32*, 361.

[24] Jones, T. B. *Electromechanics of Particles*; Cambridge Univ Pr, 2005.

[25] Morgan, H.; Green, N. G. *AC Electrokinetics: Colloids and Nanoparticles*; Research Studies Press, 2003.

[26] Castellarnau, M.; Errachid, A.; Madrid, C.; Juárez, A.; Samitier, J. Dielectrophoresis as a Tool to Characterize and Differentiate Isogenic Mutants of Escherichia Coli. *Biophys. J.* **2006**, *91*, 3937–3945.

[27] Morganti, D.; Morgan, H. Characterization of Non-Spherical Polymer Particles by Combined Electrorotation and Electroorientation. *Colloids Surfaces A Physicochem. Eng. Asp.* **2011**, *376*, 67–71.

[28] Kang, Y.; Cetin, B.; Wu, Z.; Li, D. Continuous Particle Separation with Localized AC-Dielectrophoresis Using Embedded Electrodes and an Insulating Hurdle. *Electrochim. Acta* **2009**, *54*, 1715–1720.

[29] Del Moral Zamora, B.; Colomer-Farrarons, J.; Mir-Llorente, M.; Homs-Corbera, A.; Miribel-Català, P.; Samitier-Martí, J. Combined Impedance and Dielectrophoresis Portable Device for Point-of-Care Analysis. In *Proceedings of SPIE*; 2011; Vol. 8068, p. 80680T.

[30] Lenaerts, B.; Puers, R. *Omnidirectional Inductive Powering for Biomedical Implants*; Springer Netherlands.

[31] Rashid, M. H.; González, M. H. R. V; Fernández, P. A. S. *Electrónica de Potencia: Circuitos, Dispositivos y Aplicaciones*; Pearson Educación, 2004.

Author: Beatriz del Moral Zamora
Institute: Universitat de Barcelona. Facultat de Física
Street: Martí I Franquès 1, 2a planta
City: Barcelona
Country: Spain
Email: bdelmoral@el.ub.edu

ANEX 2 –PUBLICATIONS

Authors (signature): del Moral, B.; Álvarez-Azpeitia, J.M.; Oliva, A.M.; Colomer-Farrarons, J.; Castellarnau, M.; Miribel-Català, P.Ll.; Homs-Corbera, A.; Juárez, A.; Samitier, J.

Title: Dielectrophoretic concentrator enhancement based on dielectric poles for continuously flowing samples

Book: Special Issue: Dielectrophoresis 2015

Publisher: Wiley-VCH Verlag GmbH & Co. KGaA

Beatriz del Moral Zamora[1]
Juan Manuel Álvarez Azpeitia[2]
Ana Maria Oliva Brañas[2]
Jordi Colomer-Farrarons[1]
Marc Castellarnau[3]
Pere Ll. Miribel-Català[1]
Antoni Homs-Corbera[1,2,4]
Antonio Juárez[5,6]
Josep Samitier[1,2,4]

[1]Department of Electronics, Discrete to Integrated Electronics (D2In) group, University of Barcelona, Barcelona, Spain
[2]Nanobioengineering group, Institute for Bioengineering of Catalonia (IBEC), Barcelona, Spain
[3]Research Laboratory of Electronics, Massachusetts Institute of Technology, Cambridge, MA, USA
[4]Centro de Investigación Biomédica en Red en Bioingeniería, Biomateriales y Nanomedicina (CIBER-BBN), Barcelona, Spain
[5]Microbial Biotechnology and Host-Pathogen Interaction, Institute for Bioengineering of Catalonia (IBEC), Barcelona, Spain
[6]Department of Microbiology, Faculty of Biology, University of Barcelona, Barcelona, Spain

Received September 9, 2014
Revised December 9, 2014
Accepted January 12, 2015

Research Article

Dielectrophoretic concentrator enhancement based on dielectric poles for continuously flowing samples

We describe a novel continuous-flow cell concentrator microdevice based on dielectrophoresis, and its associated custom-made control unit. The performances of a classical interdigitated metal electrode-based dielectrophoresis microfluidic device and this enhanced version, that includes insulator-based pole structures, were compared using the same setup. *Escherichia coli* samples were concentrated at several continuous flows and the device's trapping efficiencies were evaluated by exhaustive cell counts. Our results show that pole structures enhance the retention up to 12.6%, obtaining significant differences for flow rates up to 20 μL/min, when compared to an equivalent classical interdigitated electrodes setup. In addition, we performed a subsequent proteomic analysis to evaluate the viability of the biological samples after the long exposure to the actuating electrical field. No *Escherichia coli* protein alteration in any of the two systems was observed.

Keywords:
Concentrator / Dielectrophoresis / *Escherichia coli* / Lab-on-a-chip
DOI 10.1002/elps.201400433

Additional supporting information may be found in the online version of this article at the publisher's web-site

1 Introduction

DEP [1] is the term that describes the electrical force resulting from particle polarization inside a nonuniform electric field. Although DEP has been used for many years, interest in the use of this phenomenon to manipulate or characterize biological material on lab-on-a-chip (LoC) devices has been increasing recently [2–5] because of its versatility to miniaturize several analytical operations [6, 7]. DEP effect-based techniques enable the controlled and efficient manipulation of biomolecules and cells. Since the DEP force is highly associated with the intrinsic electrical properties of a particle, the medium, and the applied electrical field, it can be tuned and it is used in many applications [8] including concentrators [9, 10], and sorters [11–13] of biological material.

The application of a concentrating procedure for a biological target is part of the sample preparation protocol in a number of analytical techniques. In biomedical, food-control or environmental analyses where a small amount of target cells are found in a large sample volume, this operation is critical. In these cases, the analytical equipment needs a minimum concentration of the analyte to obtain a reliable measure. However, current procedures for sample preconcentration involve long time processes, such as culture methods [19, 20] or electrophoresis [16], are difficult to further integrate on bench-top complex analytical instruments and lack efficiency for relatively small samples. Thus, on these occasions, the

Correspondence: Beatriz del Moral Zamora, Discrete to Integrated Electronics (D2In) group, Department of Electronics, University of Barcelona, Martí i Franquès 1, 08028 Barcelona, Spain
E-mail: bdelmoral@el.ub.edu

Abbreviations: **iDEP**, insulator-based dielectrophoresis; **LB**, Luria–Bertani; **LoC**, lab-on-a-chip; **pDEP**, positive dielectrophoresis

Colour Online: See the article online to view Figs. 1, 2 and 4 in colour.

use of an efficient continuous-flow DEP-based LoC device becomes a practical option due to its swiftness and selectivity.

The objective of our work is to apply a modification to classical interdigitated electrodes DEP setups in order to improve cell concentration for biological bench-top applications. A device based on a large number of interdigitated metal electrodes placed in a microfluidic channel has been used to concentrate bacteria and other biological entities in a number of publications [14, 15]. Multiple electrode shapes have been used to better control electric field gradients [17]. One example of such works is the study by Jen et al. [19], in which HeLa cells were concentrated with 63% efficiency using DEP interdigitated chrome-gold curvy electrodes. Also, Hamada et al. [20] reported the use of interdigitated chrome electrodes to concentrate *Escherichia coli* before measuring its impedance. Another relevant work was that of Bown and Meinhart [21] who used titanium-gold electrodes to preconcentrate λ-phage DNA with an average eightfold factor. However, these devices have the limitation of generating DEP forces near the bottom of the LoC devices limiting their capabilities to trap the overall sample of interest at high flows [22–23]. To solve this issue, works based on using conductive columns to enhance the trapping capabilities have been reported [24–26]. However, these techniques imply rather complex chip fabrication and replication techniques. On the other hand, the use of insulating structures to generate electrical field nonuniformities as an alternative, or a complement, to patterned metal electrodes could solve these issues. This well-known technique can be referred to as insulator-based dielectrophoresis (iDEP) [18, 27] and it allows the generation of convenient electrical field gradients without the need to integrate complex and more numerous electrodes. Lapizco-Encinas et al. [28] concentrated and separated *E. coli* and several Bacillus species in water using isolated circular posts with a diameter of 150 μm. Similarly, Braff et al. [29] used PMMA structures to trap *E. coli* and *Bacillus cereus* at a range of direct current potentials. All these structures are especially powerful and suitable to be used to trap or concentrate such small cells and even single cells, as it has been demonstrated. As Bhattacharya et al. [30] reported it is possible to trap a single 10 μm MCF.7 breast cancer cell by means of positive DEP (pDEP). Also, Cui and Lim [31] succeeded in trapping a single 5 μm bead by adjusting negative-DEP force and the hydrodynamic forces. Thus, these structures enable higher trapping efficiencies, which permit using higher flow rates. For example, Sabounchi et al. [32] are able to preconcentrate polystyrene microspheres and *Bacillus subtilis* spores by direct current—iDEP at 30 μL/min. Also, conductive carbon electrode structures (cDEP) have shown similar effects in DEP improvement, such as the work of Elitas et al. [26] who used a DEP device based on 3D carbon electrode arrays to separate at 2 μL/min the low population of bacteria which survive antibiotic therapy. Or the work presented by Zhou et al. [33], where conductive carbon electrodes are used to separate yeast cells at a flow rate of 2.5 mL/min. However, carbon structures are an expensive technology with complicated fabrication methods. It is for that reason that the use of isolating PDMS structures to perform equivalent procedures could be a powerful technology in these applications, since it is a cheaper technology with well-known fabrication procedures [34]. Thus, using PDMS structures to perform bacteria concentration for bench-top applications could be of great interest if good efficiencies could be obtained. In this manuscript, we used pDEP, generated by alternating current, to concentrate *E. coli* in water at flow rates up to 30 μL/min, without altering cells' viability. We aim to improve concentrator methods by using iDEP structures made with PDMS. Thus, we exhaustively analyzed the experimental concentration efficiency obtained from including PDMS dielectric poles in a conventional microfluidic chip with interdigitated electrodes. In fact, by means of these structures, we also aim to obtain higher flow rates without giving up high concentration efficiencies so, reducing time invested in *E. coli* detection and avoiding lengthy culture processes by using faster and efficient DEP preconcentration. Thus, a series of concentration experiments were performed to gather consistent statistics on efficiency through exhaustive bacterium counts. Then, experiments using fluorescently tagged *E. coli* cells were performed to corroborate the effect of introducing dielectric structures in the microfluidic chamber and its benefits. Finally, a proteogram analysis [35] of the bacterial samples was performed to confirm their viability after exposure to the electrical field. By thus, ensuring the cells viability and indeed its electrical properties, they could be quantified or even measured by electrical properties in future works.

1.1 Theory

DEP [1] is the movement of an electrically neutral particle when a nonuniform electrical field is applied. When a homogeneous isotropic particle that is polarized linearly is considered, the dielectrophoretic force is defined by (1) [36, 37]:

$$F_{DEP} = \frac{1}{2} V \cdot \mathrm{Re}[\alpha^*(\omega)] \nabla |E|^2, \tag{1}$$

where E is the electrical field, V is the volume of the particle, and α is the effective polarizability (2).

$$\alpha = 3\varepsilon_0 \varepsilon_m F_{CM}, \tag{2}$$

ε_0 and ε_m are the empty permittivity and the medium permittivity respectively, and F_{CM} is the Clausius–Mosotti factor. Hereinafter, the F_{CM} sign describes the force direction. When F_{CM} is positive, the particle is attracted to an electrical field maximum (which is called pDEP). Otherwise, the particle is attracted to an electric field minimum (negative DEP). Hence, the DEP force allows control of the movement of a particle by modifying the electrical field in the medium [38]. However, it is also possible to alter this movement by varying the signal applied, by changing the electrode shape, by strategically placing dielectric structures or by modifying media properties.

Here, we used our microfluidic device and a classical one to concentrate *E. coli* cells and then evaluate their trapping

efficiency. In order to define a suitable trapping frequency, the DEP expressions were adapted to the *E. coli* geometry model. If this bacterium is considered as an ellipsoid shape with two dielectric layers [38], the adapted Clausius–Mosotti factor is as follows:

$$F_{CM_i}(\omega) = \frac{1}{2}\left(\frac{\varepsilon_p^* - \varepsilon_m^*}{\varepsilon_m^* + A_i(\varepsilon_p^* - \varepsilon_m^*)}\right), \quad (3)$$

where ε_m is the medium permittivity, ε_p is the particle permittivity, and A_i is the depolarization factor of an individual ellipsoid axe ($i = x,y,z$), which for the large axis is as follows:

$$A_x = \frac{(1-e^2)}{2e^3}\log\left(1 + \frac{e}{(1-e)-2e}\right), \quad (4)$$

where e is the eccentricity that involves the ellipsoid dimensions ("b" being the height and "a" the width):

$$e - \sqrt{(1-(b/a)^2)}. \quad (5)$$

Moreover, the depolarization factor for the shorter axis is as follows:

$$A_Z = A_y = \frac{(1-A_x)}{2}. \quad (6)$$

In a previous work [39], we reported the optimal values to manipulate *E. coli* cells by pDEP. Thus, for an aqueous medium conductivity in the range of 5.5×10^{-6} to 1.2×10^{-3} S/m, the maximum *E. coli* pDEP trapping force is around 1 MHz. Hence, this frequency was chosen for the study.

2 Materials and methods

2.1 Microfluidic chip design and fabrication

The fabrication of the microfluidic chips (Fig. 1) can be divided into three main steps, namely microchannel molding, electrode fabrication, and microfluidic chip bonding. The process followed was identical for both microfluidic chips, although the microchannels or chambers differed.

The first process was the SU8 50 (MicroChem™) masters fabrication over glass slides (Deltalab™) of 76 × 26 mm. It began with slide cleaning and an activation protocol based on piranha attack for 15 min. Then, a 50-μm high SU-8 50 (MicroChem™) was spun over the glass slides. Once exposed (Fig. 1E-1.1) and developed, the desired microchannels and pillar mold were obtained (Fig. 1E-1.2).

To replicate the microchannels, a 10:1 ratio of PDMS prepolymeric solution (Dow Corning™ Sylgard® 184) was mixed, degassed, and poured into the mold (Fig. 1E-1.3). After curing at 70ºC for 1 h, the PDMS was peeled off from the master (Fig. 1E-1.4). Obtained PDMS pillar chamber measures were additionally verified by SEM, this can be observed in Fig. 1F,

In order to fabricate the microelectrodes, a lift-off soft lithographic process was applied. Again, a piranha cleaning procedure was performed as a first step. The AZ 1512 (AZ Electronic Materials™) photoresist was chosen as a sacrificial layer. After exposure (Fig. 1E-2.1) and first development of the AZ 1512, two metal layers, formed by 20 nm of Ti and 80 nm of gold, were vapor deposited onto the surface (Fig. 1E-2.2). The final design of the electrodes was obtained by removing the AZ photoresist (Fig. 1E-2.3).

Fabricated PDMS replicas and glass slides with microelectrodes were bonded together after oxygen plasma process and alignment. After this, a cable was connected to each electrode pad (of 6 × 5 mm) by means of conductive silver paint welding. Finally, an epoxy glue mix was also applied and cured at room temperature for 60 min. Two NanoPort Assemblies were then attached in order to set the inlet and outlet connections of the chip.

2.2 Finite element simulations

Microfluidic DEP devices were simulated by a Comsol© Multiphysics 4.2a electrostatic module to investigate the capacity of the different devices to drag bacteria to electrical field maxima. For this reason, the DEP forces' intensity in the chip fluidics 3D space were studied for different designs and compared to a classical interdigitated electrodes microfluidic chamber of the same characteristics.

A small differential of each microfluidic chip (350 × 200 × 50 μm) was designed with the Solidworks CAD programme, which represented the full microfluidic chamber by applying symmetry. To simulate the applied DEP force in the chamber, the electrodes from the model were activated by two counterphased voltage signals at $V_{max}/\sqrt{2}$VRMS and $V_{min}/\sqrt{2}$VRMS and the bacteria shape and properties were introduced as global parameters so as to compute the DEP expression. Thus, the DEP forces could be obtained, as well as their dragging intensities distribution, and showing where bacteria could be attracted strongly, due to the chip design, media, and frequency used.

Then, a stationary analysis of the DEP forces was performed. The results obtained are shown in Fig. 2, where the resultant pDEP force intensity (modulus) distribution is represented for the regular chamber (Fig. 2B) and for the one with dielectric poles (Fig. 2C).

For the former, the stronger dragging and trapping effect was expected on a single plane, since the electrical field was almost fully limited to the electrode plane. In the case of the device containing the insulating structures, the electrical field gradients were modified by the poles, creating high trapping areas around them and further up from the electrode. Thus, high values of DEP force obtained around the pillars increased the dragging of bacteria toward field maximums on the 3D space. This fact can also be observed in Fig. 2C (top view), where around the poles the DEP force is ten times higher on average compared to the classic chamber, although at the electrode ends the force is similar. A higher cell trapping efficiency with this structure was

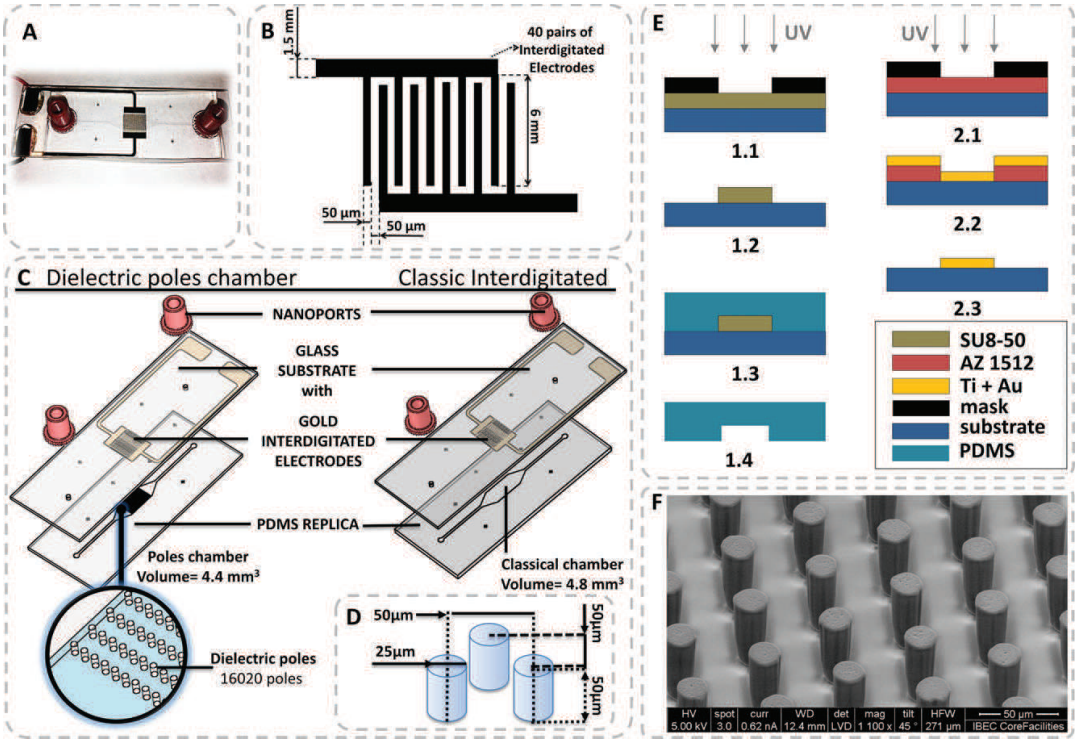

Figure 1. Microfluidic chips: overview, dimensions, and fabrication process. (A) Designed microfluidic chip. External dimension: 76 × 26 mm. (B) Electrodes representative diagram and dimensions. (C) Microfluidic chips parts. (D) Dielectric poles dimensions. (E) Fabrication protocol. (F) SEM image of PDMS pillars chamber.

therefore expected, since stronger interaction of DEP forces in the three dimensions was observed.

2.3 Bacteria culture

For the statistical and the survival tests, *E. coli* 5K cells were used. The following protocol was adopted to obtain the samples required. First, cells were grown overnight in 10 mL of Luria–Bertani (LB) broth at 37°C. Thus, the final cell concentration (estimated by performing viable cell counts in LB agar) was 10^9 cells/mL. Then, an overnight culture of *E. coli* was pelleted by centrifugation at 5000 rpm for 5 min. Cells were then re-suspended in 10 mL of DI water. The conductivity of the *E. coli* samples obtained was 11.38 µS/cm, as measured by a conductivity meter (Corning™ 441). Later, the samples were diluted to achieve 4×10^6 cells/mL. Afterwards, samples at this final concentration were separated and frozen in 1 mL collecting tubes for the experimental process.

In order to perform the fluorescence experiments *E. coli* SAR20 cells were used. These cells were obtained from CSH26 strains that were tagged by inserting a Ypf gene in the attB chromosome region [40]. Fluorescent *E. coli* SAR20 cells were treated with the same protocol as *E. coli* 5K cells, obtaining samples also of 4×10^6 cells/mL.

2.4 Experimental setup

The experimental setup is shown in Fig. 3A. The microfluidic setup was placed over an inverted microscope stage (Olympus™ IX71) attached to a digital camera (Hamamatsu™ Orca R2). Each microfluidic device was connected to a 6-port manual valve (Valco™), which controlled sample insertion with FEP tube of 0.016′ of inner diameter from IDEX™ connected to the microfluidic chip through the nanoports (Upchurt Scientific™). The valve was also connected to a 5-mL syringe filled with DI water and mounted in an infusion computer controlled micropump (Cetoni™ NEMESYS) in order to ensure a controlled continuous flow rate. The microfluidic chip gold electrodes were activated by the custom DEP driver generator defined in the Supporting Information File S.1. Finally, the custom-made device was powered by an external source (Agilent™ E3631A), so as to check the board during the experiment.

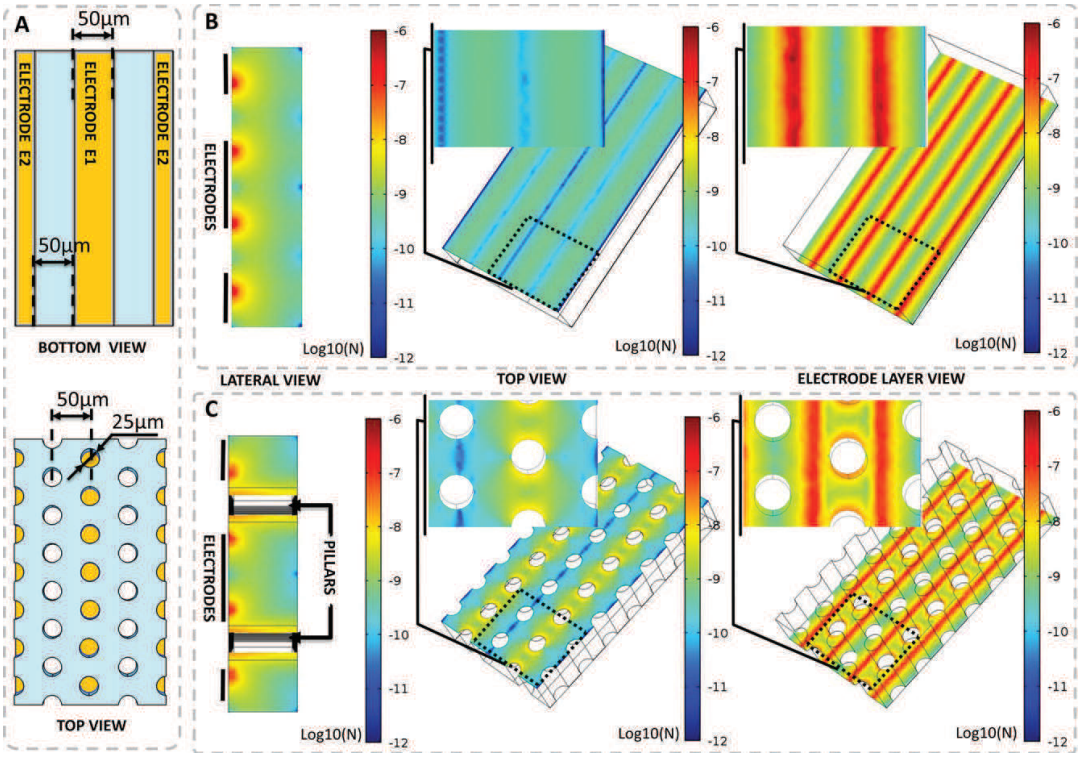

Figure 2. Chip dimensions (A) and numerical simulations of the resultant DEP force (log10(Newtons)), for the classical (B) and for the poles chamber (C). Simulation conditions: electrode E1 potential = $V_{max}/\sqrt{2}$VRMS and electrode E2 potential = $V_{min}/\sqrt{2}$VRMS. Bacteria properties $\varepsilon_m/\varepsilon_0 = 9.8$, $\varepsilon_w/\varepsilon_0 = 78$, $\varepsilon_c/\varepsilon_0 = 49.8$, $\sigma_m = 259 \times 10^{-6}$ S/m, $\sigma_w = 58 \times 10^{-3}$ S/m, $\sigma_c = 0.48$ S/m, $d_w = 8$ nm, $d_m = 50$ nm, $a = 3/2$ µm, $b = a/2$ µm.

2.5 Trapping statistics: Sample extraction protocol

The trapping efficiency of the microfluidic devices was analyzed by a series of experiments. In each four sample fractions were extracted: the original fraction (f1), the control fraction (f2), the bacteria's fraction that escaped the dielectrophoretic force (f3), and the concentrated bacteria's fraction (f4).

The sample extraction was as follows. First, a 1-mL tube of bacteria obtained from culture process (see Section 2.3) was defrosted and we collected a first 50 µL (f1) sample by using a pipette. The remaining content of the 1-mL tube was introduced into a syringe, which was connected to a valve which controls the sample injection to the microfluidic chip. This valve allows injecting bacteria in controlled loads of 50 µL. Then, a 50 µL load was injected into the chip at a continuous flow rate. During this injection, the DEP was deactivated and sample was collected at the microfluidic chip outlet. Later, a second 50 µL load was injected at the same flow rate but DEP was activated to start the bacteria concentration process. Meanwhile, the third fraction (f3) was collected at the outlet to obtain the bacteria which escaped the DEP effect. Finally, DEP was again de-activated and the last sample was collected (f4), obtaining the concentrated bacterial cells.

Afterwards, eacht fraction obtained (with 150 µL of volume after collection) was diluted again to reach 200 µL due to the cytometer specifications, and immediately frozen at −20°C. When the whole series of experiments ended, samples were defrosted, labeled with 1 µL of Green Fluorescent Nucleic Acid Stain (Invitrogen™ SYTO® 13), and counted by a cytometer (Beckman Coulter™ FC 500).

2.6 Proteomic analysis: Sample treatment and procedure

From each bacterial fraction obtained from a full DEP experimental process, 120 µL of sample was re-suspended in 240 µL of LB broth and incubated at 37ºC for 45 min. The samples were then centrifuged for 5 min at 300 rpm,

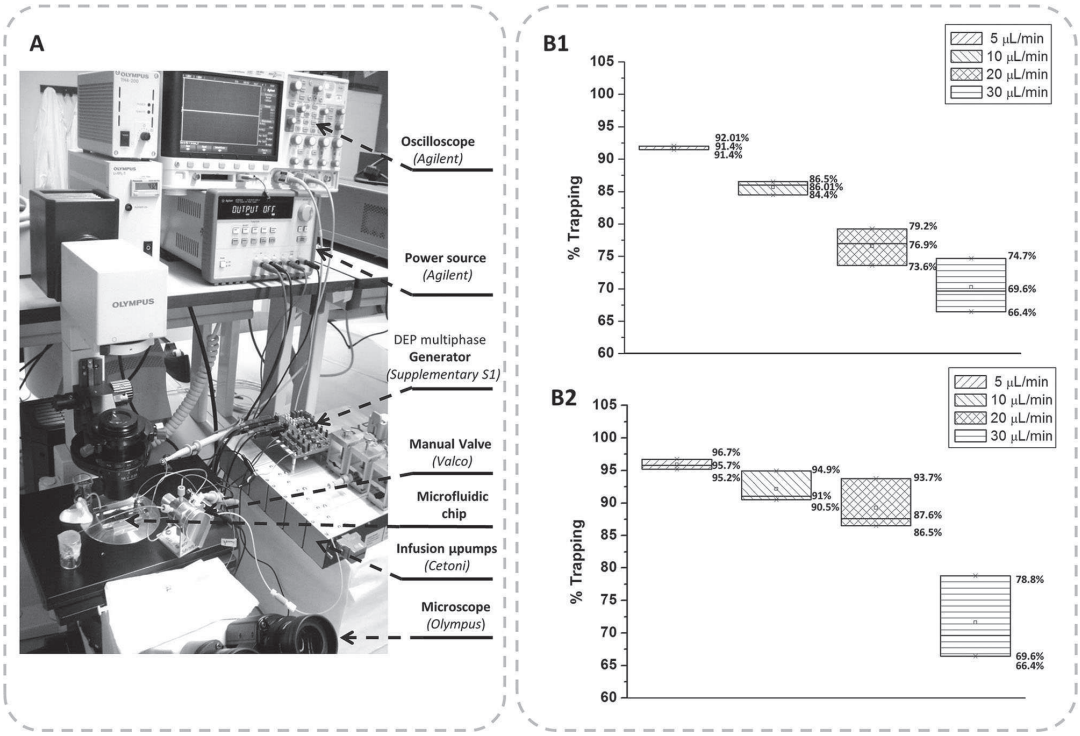

Figure 3. (A) Experimental setup. (B1/B2) Statistical results: the median, quartiles, and their values are shown. B1-labeled results are related to the classical chamber with interdigitated electrodes and B2 to the poles structure.

and the resulting pellets were re-suspended in a lysis buffer composed of 100 mM Tris/HCl (pH 8), 2 mM of EDTA, and 2% SDS. The samples from this process were then analyzed by protein assay, which consisted of verifying the protein patterns with a 15% w/v SDS-PAGE [19] .

The running gel was composed of 3.75 mL of acrylamide, 25 μL of ammonium persulfate, 5 μL of TEMED, 1.875 mL of 1.5 M of Tris (pH 8.8) as a resolving buffer, and 1.875 mL of de-ionized water. This first mixture was deposited between two glass plates in a gel caster. Soon after, some water was added to prevent air from entering. After polymerization, the water was removed by decantation, and the stacking gel was added. This gel was composed by 650 μL of acrylamide, 25 μL of ammonium persulfate, 5 μL of TEMED, 1.25 mL of 0.5 M of Tris/HCl (pH 6.8) as a stacking buffer, and 3.05 mL of DI water. Later, a 0.75 mm comb was inserted in order to create the 20 μL sample wells.

Before loading samples into wells, they were mixed with 4 μL of 5X Loading Buffer (10% w/v SDS, 10 mM DTT, 20% v/v glycerol, 0.2 M Tris/HCl (pH 6.8), and 0.05% w/v bromophenol blue), boiled for 10 min, and spun. Moreover, the first well was filled with protein marker #SM0431 in order to locate the average molecular weight of the proteins analyzed.

The protein separation on the gel was performed by electrophoresis (Bio-Rad PowerPac Basic). The electrophoresis tray was filled with 70 mL of 10X running buffer diluted in 630 mL of DI water. The gel was then introduced, and the device was set at 20 mA per gel for about 1 h. Finally, activated gels were dyed with CBB for 15 min in a rotating plate. The resultant gel was cleaned with acetic acid and DI water before being photographed by the ImageQuant LAS 4000 mini (GE HealthCare).

3 Results and discussion

In order to validate the simulation results, the statistical trapping efficiency of the two microfluidic chambers was analyzed by comparing four cases with different flow-rate conditions from 5 to 30 μL/min. Each case was repeated three times.

The two interdigitated electrodes were excited by two counterphased signals of 15 Vpp each by means of the custom-made generator described in Supporting Information File S1. Then the sample extraction protocol described in previous sections was followed. As a result, exhaustive cell counts were obtained from each individual experiment and its obtained fractions. On the basis of the cytometry results, we

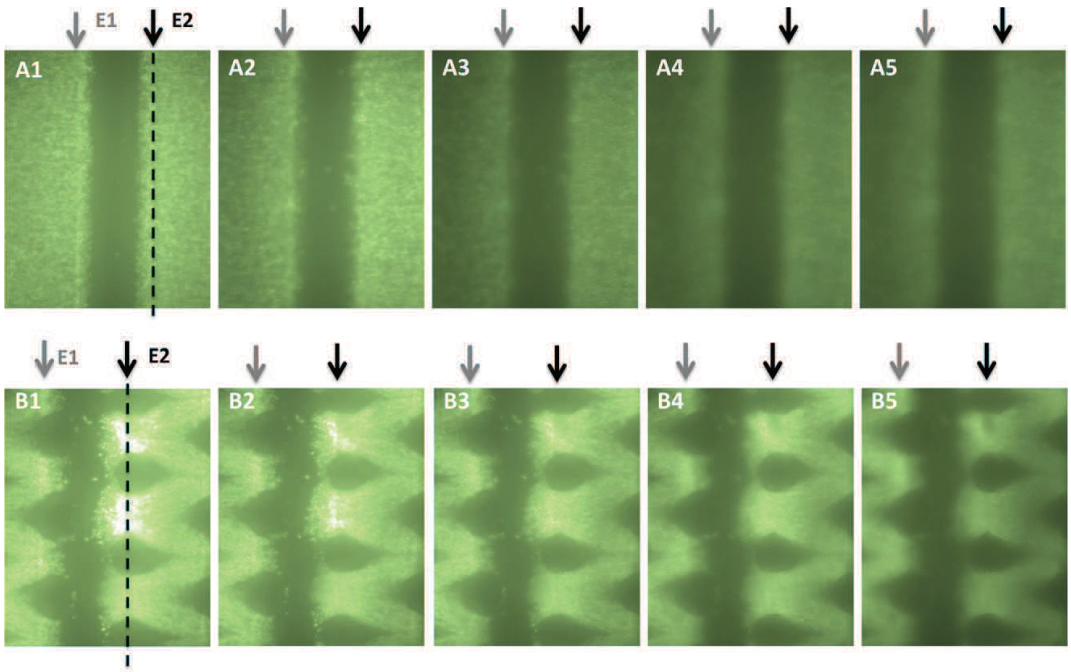

Figure 4. Fluorescence tests. "A" pictures were done with the microfluidic device with the regular chamber and "B" pictures with the poles chamber. A1 and B1 were taken at the same height, namely the electrode plane. The following numbered images (A1, A2, A3...) had a height difference of 4 μm. Thus, figures labeled with the same number (A1-B1, A2-B2, A3-B3, A4-B4, A5-B5) had the same height. As it can be seen, the poles chamber had focused bacterial cells in the higher areas (B4-B5) but this observation was not made in the classical chamber.

calculated the trapping efficiency for each experiment using the following expression (7):

$$\text{Trapping efficiency}\,(\%) = \frac{f^4}{f^2} \times 100. \tag{7}$$

The results obtained are shown in Fig. 3, where the trapping efficiency obtained for each case is shown. As a result, the poles structure showed higher efficiency (Fig. 3B2). For the lower flow rates (5 μL/min) cells were trapped with higher efficiencies in both systems. The slow flow speed helps DEP to trap a large number of cells, since in reality they are maintained for a longer time inside the chip. Furthermore, flow dynamics does not counteract DEP forces. Also, pillars structures improve DEP forces, in addition to adding physical resistance to the flow. Thus, the regular chamber (Fig. 3B1) had a median efficiency of 91.7% while the poles chamber (Fig. 3B2) showed 95.9%.

Moreover, this difference was also detected when faster flows were used. The insulating structures showed the highest efficiency (Fig. 3B2), which was due to the electric field gradients around the pillars and the resulting stronger dielectrophoretic dragging forces. The added structure also increased the effective trapping area in height, as simulated before. This poles design decreases bacteria losses at an average 44.2% for cases 5, 10, and 20 μL/min. However, the maximum average increment of trapping efficiency (12.6%) was obtained for 20 μL/min. Thus, the better performance of the presented microfluidic chip occurred when flows around 20 μL/min were used, since a high flow speed can be used without giving up efficiency. In fact, nearly all of the experiments have an efficiency greater than 87.6%. Hence, when big volumes with scarce cells need to be concentrated, this alternative could reduce diagnostic timings.

Nevertheless, at a flow rate of 30 μL/min, the flow dynamics overcame the applied DEP force, dragging cells to the outlet. Similar efficiency values were obtained for both devices. This indicates that at this speed pillars have no effect on cells and the effective trapping area is barely the electrode surface. Hence, at these flow rates experimental results indicated we reached the flow speed limits of our pillar device.

Results dependence was additionally verified by a Mann–Whitney *U*-test, comparing the obtained data from both microfluidic devices. For the analysis, data were paired by flow rate. As a result, at 5, 10, and 20 μL/min, significant differences between devices ($p < 0.05$) were detected, where efficiencies were clearly improved. On the contrary, at 30 μL/min ($p = 0.82$) differences were not so significant.

Since our results suggested that *E. coli* were trapped along the electrodes and, in the case of insulating structures, also around the pillars, we performed a fluorescence test to verify

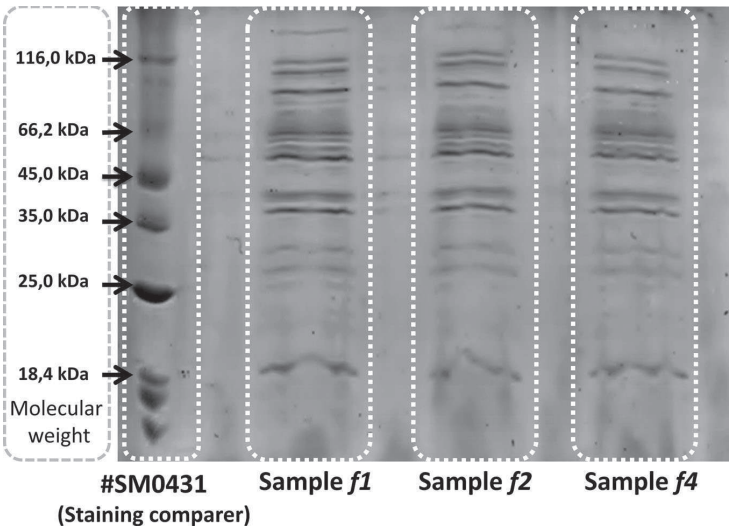

Figure 5. Resultant gel from the proteomic analysis. The left tab shows the molecular weight reference; the first column was the protein marker or the staining comparer, the three after were samples from a current experiment, which followed the statistic tests protocol, where f1 was the original fraction, f2 the control fraction, and f4 the concentrated fraction.

this hypothesis. *E. coli* fluorescence-tagged cells were introduced in the two microfluidic chips so as to visualize the trapping areas. Fifty microliters of fluoresced sample was introduced into the microfluidic device through the valve at a flow rate of 5 μL/min for 30 min, with the electrical field activated (also by two counterphased signals of 15 Vpp).

Immediately afterwards, the flow was stopped to properly observe the trapped cells. Then, by controlling the graded wheel relative to the microscope focus position, the focused fluorescent cells at different heights of the microfluidic chip were differentiated. Consequently, it was possible to observe whether cells were trapped further up from the electrode.

In the poles chamber, focused labeled cells were distinguished in all the steps (Fig. 4). By contrast, in the regular chamber, focused cells were absent at a height of 8 μm (Fig. 4A3). This observation corroborates the simulations and the statistical results, since a trapping effect close to the pillars was predicted. Thus, by adding a pillars structure we increase the dragging forces on the different planes and the trapping area, increasing the probability of dragging cells to maximums of electric field and in consequence, increasing the efficiency of our concentrator.

Finally, a third experiment was performed to conclude that the microfluidic chip with dielectric poles was suitable to be used as a bacterial cell concentrator. Since at low flow rates cells were radiated with relatively high electrical fields for a long time, a proteomic analysis of the concentrated sample was performed so as to verify the sample viability and the lack of cells irreversible stress by evaluating protein expression.

This analysis consisted of a 15% w/v SDS-PAGE (Fig. 5). The protein marks had the same intensity for all the samples (see first column for staining intensity comparison), as shown in the gel obtained. Thus, this finding indicates that protein expression was not affected by exposure to the DEP electrical field.

4 Concluding remarks

Here, we describe a novel DEP-based bacterial cell concentrator at continuous flow and compare its performance with that of one comprising classical interdigitated electrodes. The two devices, one with a regular chamber and another with a poles structure, were analyzed by exhaustive cell counts to evaluate trapping efficiency. The microfluidic devices were actuated with portable custom-made electronics, which could give rise to new integrated designs. The poles structure showed greater concentration capacity, decreasing bacteria losses at an average 44.2% for flow rates less than 20 μL/min. The concentration improvement was caused by the trapping occurring around the pillars, which was also demonstrated by simulations and fluorescence experiments. Finally, cell viability after exposure to the electrical field was verified and a protein analysis performed. No changes were noticed under these conditions.

We thank Mª Carmen Jaramillo for her help with bacterial cell treatment. This work was financially supported by the THERAEDGE Project (FP7-ICT-2007-216027), funded by the "Information and Communication Technologies" programme under the 7th Research Framework Programme of the European Union. The Nanobioengineering group is supported by the Commission for Universities and Research of the Department of Innovation, Universities, and Enterprise of the Generalitat de Catalunya (2009 SGR 505). This work was supported by Obra Social "La Caixa." CIBER-BBN is an initiative funded by the VI National R&D&i Plan 2008–2011, Iniciativa Ingenio 2010, Consolider Program, CIBER Actions and financed by the Instituto de Salud Carlos III

with assistance from the European Regional Development Fund. This material is based upon work supported by the Botín Foundation, Santander, Spain.

The authors have declared no conflict of interest.

5 References

[1] Pohl, H. A., *J. Appl. Phys.* 1951, *22*, 869–871.

[2] Pethig, R., *Biomicrofluidics* 2010, *4*, 22811.

[3] Foudeh, A. M., Fatanat Didar, T., Veres, T., Tabrizian, M., *Lab Chip* 2012, *12*, 3249–3266.

[4] Chin, C. D., Linder, V., Sia, S. K., *Lab Chip* 2007, *7*, 41–57.

[5] Vladisavljević, G. T., Khalid, N., Neves, M. A., Kuroiwa, T., Nakajima, M., Uemura, K., Ichikawa, S., Kobayashi, I., *Adv. Drug Deliv. Rev.* 2013, *65*, 1626–1663.

[6] Figeys, D., Pinto, D., *Anal. Chem.* 2000, *72*, 330 A–335 A.

[7] Stone, H. A., Stroock, A. D., Ajdari, A., *Annu. Mech.* 2004, *36*, 381–411.

[8] Demircan, Y., Özgür, E., Külah, H., *Electrophoresis* 2013, *34*, 1008–1027.

[9] Puttaswamy, S. V., Lin, C.-H., Sivashankar, S., Yang, Y.-S., Liu, C.-H., *Sensors Actuators B Chem.* 2013, *178*, 547–554.

[10] Li, M., Li, S., Cao, W., Li, W., Wen, W., Alici, G., *Microfluid. Nanofluidics* 2013, *14*, 527–539.

[11] Viefhues, M., Wegener, S., Rischmüller, A., Schleef, M., Anselmetti, D., *Lab Chip* 2013, *13*, 3111–3118.

[12] Alshareef, M., Metrakos, N., Perez, E. J., Azer, F., Yang, F., Yang, X., Wang, G., *Biomicrofluidics* 2013, *7*, 11803.

[13] Kodama, T., Osaki, T., Kawano, R., Kamiya, K., Miki, N., Takeuchi, S., *Biosens. Bioelectron.* 2013, *47*, 206–212.

[14] Feldsine, P. T., Falbo-Nelson, M. T., Hustead, D. L., *J. AOAC Int.* 1994, *77*, 58–63.

[15] Pouch Downes, F., Ito, K. (Eds.), *Compendium of Methods for the Microbiological Examination of Foods*, 4th ed., American Public Health Association, Washington, DC 2001, p. 676.

[16] Cabrera, C. R., Yager, P., *Electrophoresis* 2001, *22*, 355–362.

[17] Khoshmanesh, K., Nahavandi, S., Baratchi, S., Mitchell, A., Kalantar-zadeh, K., *Biosens. Bioelectron.* 2011, *26*, 1800–1814.

[18] Martinez-Duarte, R., *Electrophoresis* 2012, *33*, 3110–3132.

[19] Jen, C.-P., Huang, C.-T., Chang, H.-H., *Microelectron. Eng.* 2011, *88*, 1764–1767.

[20] Hamada, R., Takayama, H., Shonishi, Y., Mao, L., Nakano, M., Suehiro, J., *Sensors Actuators B Chem.* 2013, *181*, 439–445.

[21] Bown, M. R., Meinhart, C. D., *Microfluid. Nanofluidics* 2006, *2*, 513–523.

[22] Nayak, M., Singh, D., Singh, H., Kant, R., Gupta, A., Pandey, S. S., Mandal, S., Ramanathan, G., Bhattacharya, S., *Sci. Rep.* 2013, *3*, 3266.

[23] Rozitsky, L., Fine, A., Dado, D., Nussbaum-Ben-Shaul, S., Levenberg, S., Yossifon, G., *Biomed. Microdevices* 2013, *15*, 859–865.

[24] Martinez-Duarte, R., Camacho-Alanis, F., Renaud, P., Ros, A., *Electrophoresis* 2013, *34*, 1113–1122.

[25] Jaramillo, M. D. C., Martínez-Duarte, R., Hüttener, M., Renaud, P., Torrents, E., Juárez, A., *Biosens. Bioelectron.* 2013, *43*, 297–303.

[26] Elitas, M., Martinez-Duarte, R., Dhar, N., McKinney, J. D., Renaud, P., *Lab Chip* 2014, *14*, 1850–1857.

[27] Srivastava, S. K., Gencoglu, A., Minerick, A. R., *Anal. Bioanal. Chem.* 2011, *399*, 301–321.

[28] Lapizco-Encinas, B. H., Simmons, B. A., Cummings, E. B., Fintschenko, Y., *Electrophoresis* 2004, *25*, 1695–1704.

[29] Braff, W. A., Pignier, A., Buie, C. R., *Lab Chip* 2012, *12*, 1327–1331.

[30] Bhattacharya, S., Chao, T.-C., Ros, A., *Electrophoresis* 2011, *32*, 2550–2558.

[31] Cui, H.-H., Lim, K.-M., *Langmuir* 2009, *25*, 3336–3339.

[32] Sabounchi, P., Morales, A. M., Ponce, P., Lee, L. P., Simmons, B. A., Davalos, R. V, *Biomed. Microdevices* 2008, *10*, 661–670.

[33] Zhou, R., Wang, P., Chang, H.-C., *Electrophoresis* 2006, *27*, 1376–1385.

[34] Sackmann, E. K., Fulton, A. L., Beebe, D. J., *Nature* 2014, *507*, 181–189.

[35] Garner, M. M., Revzin, A., *Nucleic Acids Res.* 1981, *9*, 3047–3060.

[36] Morales, F. H. F., Duarte, J. E., Martí, J. S., *Rev. Ia Acad. Colomb. ciencias exactes, físicas y Nat.* 1936, *32*, 361–371.

[37] Jones, T. B., *Electromechanics of Particles*, Cambridge University Press, New York 2005.

[38] Morgan, H., Green, N. G., *AC Electrokinetics: Colloids and Nanoparticles*, Research Studies Press, Baldock, Hertfordshire, England 2003.

[39] Castellarnau, M., Errachid, A., Madrid, C., Juárez, A., Samitier, J., *Biophys. J.* 2006, *91*, 3937–3945.

[40] Reisner, A., Haagensen, J. A. J., Schembri, M. A., Zechner, E. L., Molin, S., *Mol. Microbiol.* 2003, *48*, 933–946.

ANEX 3–PUBLICATIONS

Authors (signature): del Moral-Zamora, B.; Punter-Villagrassa, J.; Oliva-Brañas, A.M.; Álvarez-Azpeitia, J.M.; Colomer-Farrarons, J.; Samitier, J.; Homs-Corbera, A.; Miribel-Català, P.Ll.

Title: Combined dielectrophoretic and impedance system for on-chip controlled bacteria concentration: Application to Escherichia coli

Book: ELECTROPHORESIS. Special Issue: Focus on the London Dielectrophoresis 2014 Meeting

Publisher: Wiley-VCH Verlag GmbH & Co. KGaA

Beatriz del Moral-Zamora[1]
Jaime Punter-Villagrassa[1]
Ana M. Oliva-Brañas[2]
Juan Manuel Álvarez-Azpeitia[2]
Jordi Colomer-Farrarons[1]
Josep Samitier[1,2,3]
Antoni Homs-Corbera[1,2,3]
Pere Ll Miribel-Català[1]

[1]Department of Electronics, University of Barcelona, Barcelona, Spain
[2]Nanobioengineering Group, Institute for Bioengineering of Catalonia (IBEC), Barcelona, Spain
[3]Centro de Investigación Biomédica en Red en Bioingeniería, Biomateriales y Nanomedicina (CIBER-BBN), Zaragoza, Spain

Received September 19, 2014
Revised February 4, 2015
Accepted February 9, 2015

Research Paper

Combined dielectrophoretic and impedance system for on-chip controlled bacteria concentration: Application to *Escherichia coli*

The present paper reports a bacteria autonomous controlled concentrator prototype with a user-friendly interface for bench-top applications. It is based on a microfluidic lab-on-a-chip and its associated custom instrumentation, which consists of a dielectrophoretic actuator, to preconcentrate the sample, and an impedance analyzer, to measure concentrated bacteria levels. The system is composed of a single microfluidic chamber with interdigitated electrodes and an instrumentation with custom electronics. The prototype is supported by a real-time platform connected to a remote computer, which automatically controls the system and displays impedance data used to monitor the status of bacteria accumulation on-chip. The system automates the whole concentrating operation. Performance has been studied for controlled volumes of *Escherichia coli* samples injected into the microfluidic chip at constant flow rate of 10 μL/min. A media conductivity correcting protocol has been developed, as the preliminary results showed distortion of the impedance analyzer measurement produced by bacterial media conductivity variations through time. With the correcting protocol, the measured impedance values were related to the quantity of bacteria concentrated with a correlation of 0.988 and a coefficient of variation of 3.1%. Feasibility of *E. coli* on-chip automated concentration, using the miniaturized system, has been demonstrated. Furthermore, the impedance monitoring protocol had been adjusted and optimized, to handle changes in the electrical properties of the bacteria media over time.

Keywords:
Autonomous device / Bacteria concentrator / Dielectrophoresis / *Escherichia coli* / Impedance analysis
DOI 10.1002/elps.201400446

1 Introduction

In the last few years, the electrical properties of cells and pathogens have been used to explore new methods of manipulation and characterization, such as dielectrophoresis (DEP) [1] or impedance analysis (IA) [2, 3]. For instance, DEP has been recently used to control stem cells to form embryonic bodies in shorter time [4] and Fatoyinbo et al. [5] have measured biophysical parameters of cells (cytoplasmic conductivity, membrane conductivity, and cell-wall conductivity) by analyzing its cells' DEP behavior. Moreover, IA was also advantageous to detect ovarian cancer cells SKV3 [6] or to detect insulin levels in blood serum [7] so as to diagnose diabetes or trauma. We present a miniaturized and compact specific solution to concentrate bacteria in a controlled manner using a fully automated instrument combining DEP and IA.

Bacteria concentration is a time-consuming procedure in regular microbiology laboratory practices that involves cell-culturing processes [8, 9] to obtain a significant sample. This could be improved by using DEP as a means of concentration in tiny fluidic spaces. DEP refers to the force experienced by a particle inside a nonuniform electric field [10, 11] and is a convenient, rather selective, handling method that has been applied in many biological fields and in lab-on-a-chip (LoC) devices [12–14]. An example of this is the work reported by Lapizco-Encinas et al. [15], where several types of bacteria in water were concentrated and separated by DEP induced by insulator-based structures (iDEP), or in the paper presented by Braff et al. [16], where bacteria were successfully DEP trapped in PMMA constructs. DEP selectivity has also been repeatedly reported as a benefit for sample preparation, since it allows isolation of the desired cell or pathogen based on their electric and geometric properties [17–19]. As

Correspondence: ME Jaime Punter-Villagrasa, Department of Electronics, University of Barcelona, Martí i Franquès 1, 08028 Barcelona, Spain
E-mail: jpunter@el.ub.edu

Abbreviations: ADC, analog-to-digital converter; **DEP**, dielectrophoresis; **FRA**, frequency response analyzer; **IA**, impedance analysis; **IDE**, interdigitated electrode; **LoC**, lab-on-a-chip

Colour Online: See the article online to view Figs. 1, 2, 4 and 5 in colour.

an example, Moon et al. [19] used DEP to separate and detect circulating tumor cells, whose size and resistance to filtering shear stress presented significant differentiating properties, from regular blood cells. This also becomes an advantage in the case of environmental samples, where soil particles with the same bacteria size are also present and could not be eliminated by filtration or centrifugation. This has also been solved by using DEP [20], taking advantage of its selectivity by cell electrical properties. Hence, we used DEP here for concentration purposes.

On the other hand, current bacteria-detection protocols are expensive in terms of equipment and time, typically requiring several days to obtain results [21, 22]. Techniques such as pathogenic-specific antibody-coated magnetic beads [23, 24] or hybridization of DNA fragments of bacteria [25] have shown to improve the analysis time down to several hours, but they still need complex equipment. This could be improved by using IA. Impedance frequency dependence, which is related to the electrical conductivity and permittivity properties of the material, was reported as an effective solution to characterize cells and their behavior, also in LoC devices [26]. Some publications have reported the use of IA technique to control bacterial growth or to detect its presence [27]. One example of such work is the paper presented by Dweik et al. [28], where bacterial presence was rapidly detected by measuring the antibody/antigen bonding using IA in the 100 Hz to 10 MHz range. Another example is the work of Grossi et al. [29], where the quantity of bacteria during a culture process was detected by impedance measured at 200 Hz using a sinusoidal signal with a 50 mV amplitude.

The combination of DEP and IA [3, 30] in a single equipment based on LoC and microfluidic technologies allows to develop a practical bench-top device. In recent years several biosensors and applications aiming for the successful combination of both techniques have been presented. Hamada et al. [3] presented a bacterial detection device combining both positive DEP and negative DEP with dielectrophoretic impedance measurement. The biosensor relied on a pair of interdigitated electrodes (IDEs) for separate DEP concentration and dielectrophoretic impedance measurement, while using commercial devices to operate the application. The cellular solution conductivity varies through time, which affects the impedance measurement, which has not been considered, and measurement instability produced by the magnitude of DEP voltage has been reported. Dastider et al. [30] have designed an impedance biosensor for the specific detection of *Esherichia coli* O157:H7 combining DEP and IA techniques at 2 μL/min flow rate, which is relatively low. This work used different IDEs for cellular separation and detection purposes. The detection IDE was functionalized with polyclonal anti-*E. coli* antibodies for specific detection of *E. coli* O150:H7, removing versatility of the device. Moreover, the presented results for cells' concentration detection, based on impedance measurements, did not consider the solution conductivity variations, as well as the influence of DEP voltages on the impedance measurement.

Our work presents a completely customized equipment for a quick and easy way to concentrate bacteria with DEP technique at relatively high flow rates [31, 32], while monitoring its concentration by means of IA technique in a real-time scenario. It addresses the issues associated with the combination of these techniques by simplifying the equipment but also by trying to solving some issues generally avoided, to the best of our knowledge in other scientific works.

The device, with its main components, is presented in Fig. 1. It is composed of a customized electronic module and an LoC. The flowing bacteria sample is preconcentrated through the generated DEP generation and concentration is measured through IA monitoring, with a four-electrode sensor topology, embedded on a single microfluidic chamber. The electronic module is supported by a real-time platform for continuous concentration monitoring, connected to a remote computer through a standard Ethernet connection, which enables the system configuration and data display. First, it allows automated functionalities, such as multiplexing signals between the DEP generator and the IA analyzer in the microfluidic chip, in order to avoid DEP voltages disturbance of IA measurement, and auto-scale of the electronic instrumentation gains when necessary, for better signal acquisition. Second, it is connected to a remote computer with a user-friendly front-end user panel, where the system user can configure the experiment variables, such as measurement time for signal multiplexing, signal operation frequency, and output gain, while displaying the impedance measurements related to actual bacteria concentration level.

The solution presented controls, in an automated way, the bacteria concentration, and monitoring process and has been validated for *E. coli*, which presents pathogenic variants that cause morbidity and mortality worldwide [33]; therefore being a topic of interest. *E. coli* is one of the main antimicrobial-resistant pathogens for healthcare-associated infections reported to the National Healthcare Safety Network [34], being the primary cause of widespread pathologies such as significant diarrheal and extraintestinal diseases [33] or urinary tract infections [35]. Furthermore, *E. coli* can be found as a bacterial food contamination [21] and causes avian colibacillosis, one of the major bacterial diseases in the poultry industry and the most common avian disease communicable to humans [36].

The aims of our study are (i) to prove the feasibility of DEP generator and IA analysis combination for controlled concentration using a single equipment together with a single microfluidic chip; (ii) to establish a protocol for autonomous concentration procedure; and (iii) to develop a complete electronic equipment with an electronic instrumentation, embedded software control, and user interface for a complete autonomous and reliable bacteria concentrator device, based on DEP generator and IA technique.

This novel, specific device has been proven as a robust and reliable automated system and protocol for bacteria controlled concentration. It will provide the scientific community with a rapid tool for bacteria presence detection, by avoiding

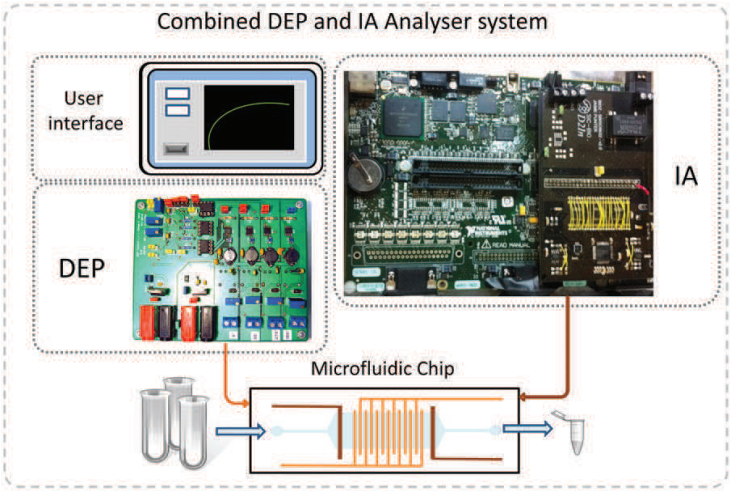

Figure 1. Combined system overview.

previous slow preparations in preconcentration and culture processes, reducing procedure times for a faster diagnosis and treatment.

2 Theory

2.1 The dielectrophoretic effect

DEP [11] defines the movement of an electrically neutral particle when a nonuniform electric field is applied. If the particle is considered homogeneous and isotropic and is polarized linearly, then the dielectrophoretic force is defined by Eq. (1) [37, 38]—where V is the volume of the particle; E is the electric field; and α is the effective polarizability, which is defined by the expression (2):

$$F_{\mathrm{DEP}} = \frac{1}{2} V \cdot Re\left[\alpha^*(\omega)\right] \nabla |\vec{E}|^2 \tag{1}$$

$$\alpha = 3\varepsilon_0 \varepsilon_m F_{\mathrm{CM}}, \tag{2}$$

where ε_0 and ε_m are the vacuum permittivity and the medium permittivity, respectively, and F_{CM} is the Clausius–Mosotti factor. The F_{CM} sign describes the force direction: if F_{CM} is positive, the particle is attracted to an electrical field maximum (which is called positive DEP or p-DEP) and if negative, to an electrical field minimum (negative DEP or n-DEP). Hence, the DEP force allows control of the movement of a particle by varying the applied signal, changing the electrode shape, placing dielectric structures, or modifying media properties. Here we used a pair of interdigitated gold electrodes to preconcentrate *E. coli* cells. In order to define the suitable trapping frequency, an *E. coli* geometry model is considered. This bacterium is approximated to an ellipsoid shape with two dielectric layers [10], which modifies the Clausius–Mosotti factor expression:

$$F_{\mathrm{CM_i}}(\omega) = \frac{1}{2} \left(\frac{\varepsilon_p^* - \varepsilon_m^*}{\varepsilon_m^* + A_i\left(\varepsilon_p^* - \varepsilon_m^*\right)} \right), \tag{3}$$

where ε_m is the medium permittivity; ε_p is the particle permittivity; and A_i is the depolarization factor of an individual ellipsoid axe ($i = x, y, z$), where e is the eccentricity that involves the ellipsoid dimensions (where "b" is the height and "a" the width):

$$A_x = \frac{(1-e^2)}{(2e^3)} \log\left(1 + \frac{e}{(1-e) - 2e}\right) \tag{4}$$

$$A_z = A_y = \frac{(1 - A_x)}{2} \tag{5}$$

$$e = \sqrt{1 - \left(\frac{b}{a}\right)^2}. \tag{6}$$

The representation of expression (3) showed that the optimal frequency to manipulate *E. coli* cells by p-DEP is 1 MHz as we know from previous studies of the group [39,40]. This frequency was therefore chosen for the preconcentrating stage.

2.2 Impedance and available measurement methods

The bioimpedance [41, 42] can be measured as the voltage response of a biological material to the application of a current bias signal, and is defined by the Ohm's law. The methods of impedance measurement are classified by the number of electrodes used: two-, three-, and four-electrode methods. The difference among methods resides in how bias current signal is applied and how the sensor voltage signal response is read.

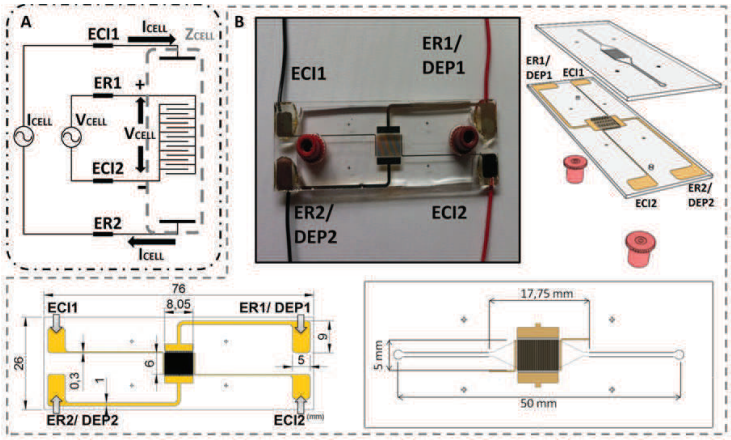

Figure 2. (A) Four-electrode impedance measurement method. (B) Designed microfluidic chip. ECI1–ECI2 are the current injection electrodes, ER1–ER2 are the reading electrodes, and DEP1–DEP2 are referred to electrodes where DEP is applied.

A two-electrode configuration is the basic topology, defined by the working electrode, where bias signal is applied, and the reference electrode, which tracks the bias current signal and provides a reference for the voltage measurement. However, as the current bias signal flows through the reference electrode, this topology entails some problematic behavior as the voltage reference is distorted due to electrode polarization. In order to avoid this effect, the three-electrode topology adds a third electrode to supply the bias current signal, while the reference electrode remains as a voltage reference.

Although this is an improvement, the impedance measurement with this topology can be distorted due to the working electrode impedance polarization, as the current bias signal is directly applied where the single-ended voltage measurement signal is read. In this paper, the four-electrode method was used (Fig. 2A, electrodes ER1, ER2, ECI1, ECI2), which was composed of two current injection electrodes and two voltage reading electrodes, as this electrode topology avoids electrode polarization distortion in impedance measurement due to a complete differential voltage measurement [43].

3 Materials and methods

3.1 Microfluidic chip design and fabrication

The designed microfluidic chip design is showed in Fig. 2B. This had two IDEs, which were shared between the DEP generator and impedance analyzer readout electronics, and two lateral electrodes, which were used to inject the necessary current so as to obtain the impedance measure. The IDEs were formed by 40 pairs of 6 mm × 50 μm electrodes separated by 50 μm. The lateral electrodes (6 mm x 300 μm) were separated by 200 μm from the interdigitated ones. These electrodes were attached to a PDMS microfluidic chamber with a volume of 4.8 μL. The fabrication of the microfluidic chips followed a protocol based on three main steps: microchannel molding, electrode fabrication, and microfluidic chip bonding.

First, SU8 50 (MicroChem) masters were fabricated over glass slides (Deltalab) and PDMS replicas were created. In order to do this, the glass slide was cleaned and activated by Piranha attack for 15 min. Then a 50-μm-high SU-8 50 (MicroChem) was spun over the slides. They were later exposed and developed so as to obtain the desired microchannels. Afterward, a 10:1 ratio of PDMS prepolymeric solution (Dow Corning Sylgard184) was mixed, degassed, and poured into the mould to replicate the microchannels. Finally, the PDMS was cured at 70°C for 1 h and peeled from the master.

Second, in order to fabricate the microelectrodes over a set of the LoC sealing glass slides (Deltalab), a lift-off soft lithographic process was used. AZ 1512 (AZ Electronic Materials) photoresist was chosen as a sacrificial layer in this process. First, a Piranha cleaning procedure was performed over the glass slides. Later, AZ 1512 was spun on these slides, exposed, and developed. Then, two metal layers, 20 nm of Ti and 80 nm of gold, were vapor-deposited sequentially. The electrode structures were finally obtained by removing the AZ photoresist.

As a final microfluidic chip fabrication step, once the PDMS replica and the microelectrodes were finished, both parts were assembled to create a sealed structure. First, the surfaces were cleaned using an oxygen plasma process. Hereinafter, the PDMS channels were aligned and attached to the glass substrate. Later, cables were welded to each electrode pad using conductive silver paint and mechanically strengthened using an epoxy glue mix, later cured at room temperature for 60 min. Finally, two NanoPort Assemblies were attached in order to set the inlet and outlet fluidic connections.

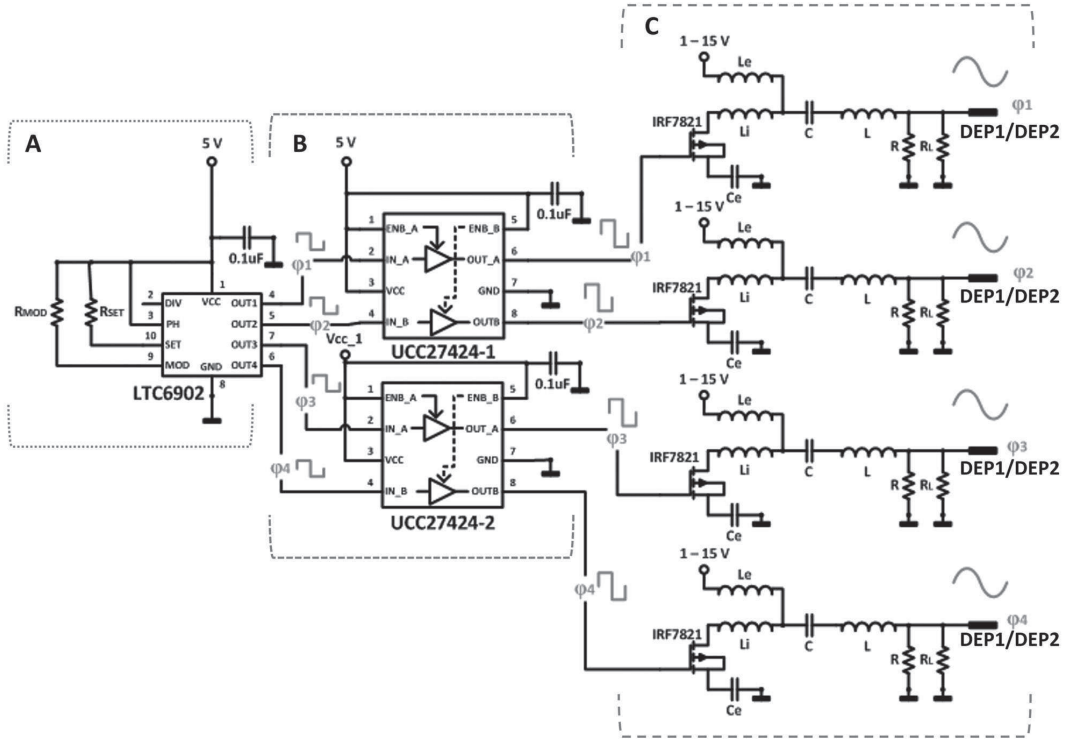

Figure 3. Schematic of the DEP module. (A) Square signal generator. (B) Power driver. (C) Class E amplifier.

3.2 Combined DEP and IA device

3.2.1 Dielectrophoretic signal generator electronics

The designed dielectrophoretic signal generator module is presented in Fig. 3. Four channels with different phases (0°, 90°, 180°, 270°), which could be connected in different ways to the electrodes DEP1 and DEP2, were defined so as to add versatility to the board in dielectrophoretic terms. Each channel generates a sinusoidal signal at 1 MHz with variable output voltage from 1 to 15 Vpp (peak to peak) to control the DEP force intensity, and is composed of three modules: (i) A square signal generator that provides four shifted and frequency stable signals (A); (ii) a power driver that boosts the signal from the previous module so as to activate the following stage (B); (iii) a class E amplifier, which generated the DEP sinusoidal signal (C).

The first module, the square signal generator, is based on the LTC6902 (Linear Technology). The synchronized outputs are shifted $\varphi 1 = 0°$, $\varphi 2 = 90°$, $\varphi 3 = 180°$, and $\varphi 4 = 270°$, respectively. Their output frequency is selectable by an external resistor (R_{SET}), following the Eq. (7) where ($N = 10$ is related to frequency working range and $M = 4$ is the number of active outputs),

$$f_{out} = \frac{10\ \text{MHz}}{N \cdot M} \left(\frac{20\text{k}\Omega}{R_{set}} \right). \tag{7}$$

LTC6902 outputs have a supplying limit of 400 μA. Hence, a power driver is used to increase the current capabilities. An UCC27424 (Texas Instruments) is chosen for this purpose. This device boosts the current levels of the input signal up to 4 A, which is sufficient current to drive the final module. This module is a class E amplifier that generates the necessary sinusoidal signals to apply DEP. This amplifier configuration generates high-frequency signals with stable output voltages [44– 46] by injecting a square high current control signal.

The class E amplifier is composed of an inductor Le, a capacitor Ce, and a resonance tank formed by the inductor L and the capacitor C. The L–C tank generates a 1 MHz sinusoidal signal by using the 1 MHz square signal from the previous modules. The circuit parameters (Le, Ce, C, L) were configured in function of the necessary output frequency, the output impedance, and the equivalent resistance of the

microfluidic chip. Thus, four independent channels perfectly synchronized at φ1, φ2, φ3, and φ4 are obtained.

3.2.2 Impedance analyzer electronics

A fully customized electronic circuit was specifically designed to carry out the IA experiments. As previously stated, the microfluidic device impedance measurement is based on the four-electrode topology. A four-electrode method is composed of two current injection (ECI1 and ECI2) electrodes and two voltage reading (ER1 and ER2) electrodes. The main advantage of this system is that electrode impedances are cancelled, obtaining a more reliable measure. The circuit specifications were defined taking into account the sample media impedance, and considering the microfluidic device characteristics and the frequency ranges where bacterium could be discriminated [47, 48].

The impedance analyzer architecture consists of two modules: the current injection module (CI in Fig. 4B) that provides a frequency configurable voltage sinus signal (V_{RS}) that is converted to a current signal (voltage-to-current converter circuit) to bias/drive the current injection electrodes ECI1 and ECI2. An instrumentation amplifier (IA) senses the differential voltage between the reading electrodes ER1 and ER2 (V_{IS}).

The second module, signal digitalization and post-processing (SDPP in Fig. 4A), calculates the impedance measurement through the voltage signals provided by the previous stage, and automatically controls the hardware configuration. This module is composed of a real-time platform sbRIO9632 (National Instruments) with an embedded software for data processing and hardware control. A signal conditioning stage converts voltage signals from a bipolar single-ended signal to a unipolar differential signal to be processed by an analog-to-digital converter (ADC).

The first module (CI), current Injection, is based on a signal generator AD9833 (Analog Devices) and a voltage-to-current converter. The signal generator AD9833 provides a stable voltage signal with a wide variable frequency range, 0 to 12.5 MHz, which is controlled by an SPI communication protocol. The voltage-to-current converter is a modified Howland cell based on AD8066 (Analog Devices) operational amplifiers (OA1 and OA2) that guarantee a wide bandwidth and a high slew rate while maintaining a low spectral noise and a low offset performance. The Howland cell uses R_{SET} and the reference signal (V_{RS}) amplitude to define a stable current signal (I_{OUT}) at the output of the circuit (8) regardless of the connected load.

$$I_{OUT} = \left(\frac{1}{R_{SET}}\right) V_{RS} \tag{8}$$

The differential voltage between ER1 and ER2 electrodes is acquired by means of the instrumentation amplifier (IA) INA163 (Texas Instruments), which allows a wide bandwidth with a low spectral noise and low total harmonic distortion. The measured voltage (signal V_{IS}) is related to the differential voltage between the reading electrodes (ER1 and ER2), G being the instrumentation amplifier gain. This V_{IS} signal is then adapted and processed by the SDPPM module in order to extract the impedance of the media.

$$V_{IS} = G \cdot (V_{ER1} - V_{ER2}) \tag{9}$$

The second module (SDPP), signal digitalization and post-processing, consists of a 12-bit, dual, low-power ADC ADC12D040 (Texas Instruments), capable of converting both analog input signals at 40 MSPS simultaneously. Twelve-bit resolution does not represent a significant drawback in the final system resolution, as V_{RS} is scaled to the full-range ADC analog input and the system provides a real-time gain auto-scale for the instrumentation amplifier gain G. The analog inputs are converted from single ended to differential with a differential amplifier (DA) AD8138 (Analog Devices), with a high slew rate with low distortion and input noise. The impedance measurement is carried out with a digital lock-in based on the frequency response analyzer (FRA) approach [49]. The FRA is a real-time mathematical processing system, embedded in the 400 MHz microprocessor from the real-time platform sbRIO9632, which adopts sine and cosine signals related to V_{RS}, and by means of two multipliers and a filter stage, the real (V_{REAL}) and imaginary (V_{IM}) components values (10) of the measured signal V_{IS} are obtained (Fig. 4C). The key measurement in our work is the impedance magnitude ($|Z_{CELL}|$) (Eq. (11)). This value is calculated based on the V_{REAL} and V_{IM} components.

$$V_{REAL} = \frac{1}{2V_{RS}} \cdot V_{IS} \cdot \cos(\varphi_{IS}) \; ; \; V_{IM} = \frac{1}{2V_{RS}} \cdot V_{IS} \cdot \sin(\varphi_{IS}) \tag{10}$$

$$|Z_{CELL}| = \left(\frac{2\sqrt{{V_{REAL}}^2 + {V_{IM}}^2}}{|V_{RS}|^2}\right) \cdot R_{SET} \tag{11}$$

For accurate hardware control, the real-time platform sbRIO9632 has a FPGA Spartan-3 (Xilinx), which allows us to provide steady clock signals, needed on the instrumentation, which can be automatically adjusted, allowing complete real-time control of the chip electrodes multiplexing. As stated in Section 2.1, the microfluidic chip had two IDEs, which were shared between the DEP generator and the IA readout electronics. When an IA measurement was done the DEP generator was disconnected, suspending the trapping process. If this process was not properly timed, bacteria already trapped would be lost in the process, so the real-time control allowed an optimized timing process minimizing the bacteria loss. Moreover, the disconnection of DEP voltage signals contributes to a better bacterial concentration monitoring avoiding distortion and instability on the IA measurement. The IA process had been programmed and tested to last for a period of the applied current signal, plus 1 ms for multiplexor switching times and stabilization. In addition, real-time platform allows complete parallel signal acquisition for all the frequency ranges, and the development of an embedded hardware control, such as R_{SET} multiplexed auto-scale, instrumentation amplifier gain G auto-scale, and signal generator automatic frequency sweep. This real-time embedded

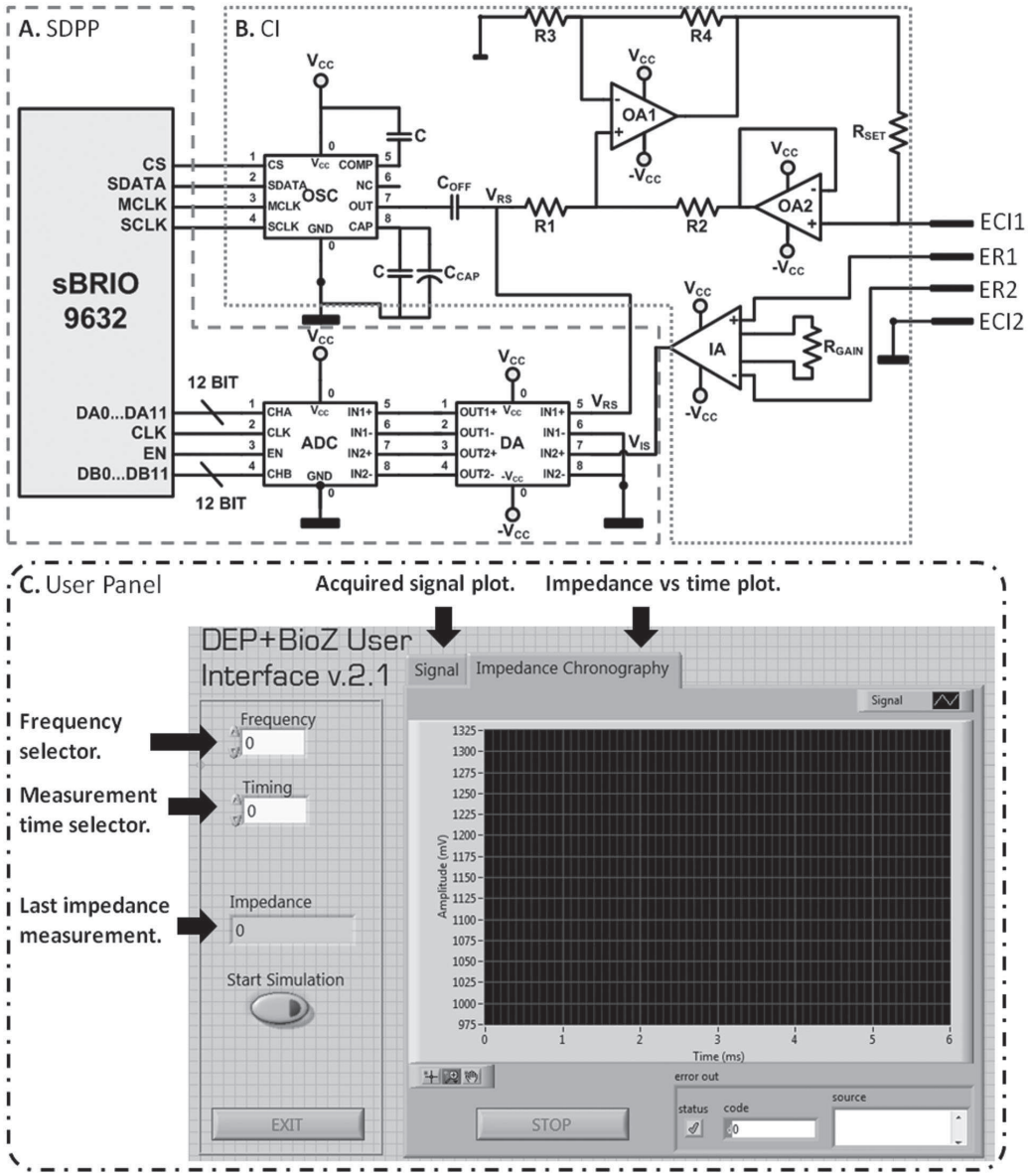

Figure 4. Schematic of the IA module. (A) Signal digitalization and postprocessing module (SDPP). (B) Current injection module (CI). (C) Front-end user panel for experiments control and data displaying.

hardware control represents the basic features of an automated and complete FRA approach. The real-time platform allows the system configuration and data display, with a user-friendly front-end user panel (Fig. 4C), by means of an external computer connected to the platform with a standard Ethernet connection.

3.3 Bacteria culture

A laboratory sample formed by *E. coli* 5K strains (genotypes: F^-, hdsR, hdsM, thr, thi, leu, lacZ) was grown overnight in 10 mL of Luria–Bertani broth at 37°C. The achieved cell concentration (estimated by performing viable cell counts

in LB agar) was 10^9 cells/mL. Then, the *E. coli* culture was pelleted by centrifugation at 5000 rpm for 5 min. Bacteria were then resuspended in 10 mL of DI water. Finally, the samples were diluted (final concentration of 2×10^7 cells/mL) and frozen in 1 mL collecting tubes for storage purposes.

3.4 Conductivity measurements

As *E. coli* concentration was measured by means of IA, bacteria samples' conductivity was monitored while in vitro a major factor in IA reliability, using a commercial bench-top conductivity meter Corning 441. Prior to the experiments, bacteria samples were diluted in DI water with a conductivity of 8.2×10^{-5} S/m, but the conductivity of the samples at the time of the experiment, after the process of storage and thawing, was subject to variations. A sample conductivity analysis had to be done at the beginning of the experiment. The conductivity meter probe was calibrated and introduced into the 1 mL collecting tubes until it was totally covered by the bacteria sample.

3.5 Experimental setup

The microfluidic chip was placed over an inverted microscope stage (Olympus IX71) connected to a digital camera (Hamamatsu Orca R2). Moreover, the microfluidic chip was connected to a six-port manual valve (Valco). This valve was also connected to a 5 mL syringe filled with DI water (8.2×10^{-5} S/m) and placed on an infusion micropump (Cetoni NEMESYS) so as to obtain a continuous flow rate. The microfluidic chip's gold electrodes were connected to the custom combined DEP and IA device.

4 Results and discussion

The designed combined device was validated by a series of *E. coli* concentration and impedance measurement tests. First of all, so as to validate the system as an autonomous bacteria concentrator, and study the effect of real-time monitoring by means of IA measurement, *E. coli* was continuously injected through the valve to the microfluidic chip at a 5 μL/min flow rate, and preconcentrated by DEP by two counter-phased signals of 15 Vpp. In addition, the impedance module was programmed to proceed with a 3-ms impedance measurement every 30 s meanwhile DEP module was continuously trapping bacteria. As a first approach, the conductivity of the solution has not been corrected to study the effect its variations over time on the IA measurement. Different tests for different applied current signal frequencies were done. Taking into consideration the electronics and microfluidic chip design, impedance measurement was performed at continuous alternating current of 10 μA in the 500 Hz to 5 kHz frequency range, where bacterium could be discriminated [47, 48] and evaluated using 100 Hz spaced sampling intervals.

The measured bioimpedance ($|Z|$), depicted in Fig. 5A, clearly shows a decreased impedance as the trapped bacteria concentration increases, regardless of the frequency. This behavior was clearly explained by the conductivity changes taking place in bacteria samples over time. Measured conductivity was recorded periodically in-tube during the experiments showing a rise from 0.5×10^{-3} to 2.5×10^{-3} S/m until it stabilized. This conductivity change, related to the original sample prior to the trapping process, may be translated into a theoretical variation in impedance. This estimated impedance, related to measured bacteria sample in-tube conductivity, was calculated considering the microfluidic chip electrodes' geometric characteristics. In Fig. 5B impedance variation ($\Delta|Z|$) through time for the measured on-chip impedance, during the trapping process, and for the estimated on-tube impedance are shown.

Results show a very similar behavior through time of both measurements. Acquired data variations through time for the first 40 min, before conductivity stabilization, were $-52.41\ \Omega$/min for measured impedance and $-54.79\ \Omega$/min for conductivity related impedance, which confirms that the first impedance measurements are related to bacteria sample conductivity rather than trapped bacteria concentration, underlining the need for a media conductivity correcting protocol.

A 2D finite element method based study with Multiphysics software (Comsol) further shows the dominating effect of sample conductivity changes on the bioimpedance measurements when left uncontrolled. *E. coli* 5 K physical and electrical properties were defined for the different model layers ($\sigma_{wall} = 0.68$ S/m, $\varepsilon_{r\_wall} = 74$, $\sigma_{membrane} = 5 \times 10^{-8}$ S/m, $\varepsilon_{r\_membrane} = 9.5$, $\sigma_{cytoplasm} = 0.19$ S/m, $\varepsilon_{r\_cytoplam} = 49.8$). Then different medium conductivities were defined, as well as the applied potential to the external lateral electrodes. Current conservation and an initial state of potential 0 were applied for all the layers. Afterward, an adaptive physical controlled and extra fine mesh was applied. Finally, a frequency domain analysis at 1.7 kHz was performed. Thus, surface current density (ec.normJ) of bacteria was obtained (Fig. 5C andD). From the analysis of the obtained simulations, we could assure that in case of a single bacteria diluted on a buffer with a conductivity which varies from 0.5×10^{-3} to 2.5×10^{-3} S/m, current density is 99.9% located outside the bacteria. Hence, measured impedance is totally related to sample buffer conductivity rather than bacteria concentration (Fig. 5C). Controlling buffer conductivity to be stable and at the levels of Milli-Q water, around 8.2×10^{-5} S/m, current density is mainly located in the cell membrane (Fig. 5D) and impedance variation related to the quantity of trapped bacteria.

Hence, when the cells' media is not controlled by cleaning processes, impedance variations are strongly related to changes in the conductivity of the media due to bacteria [50, 51]. To solve this issue, which is not confronted in other works to the best of our knowledge, an automated periodic cleaning process was implemented as part

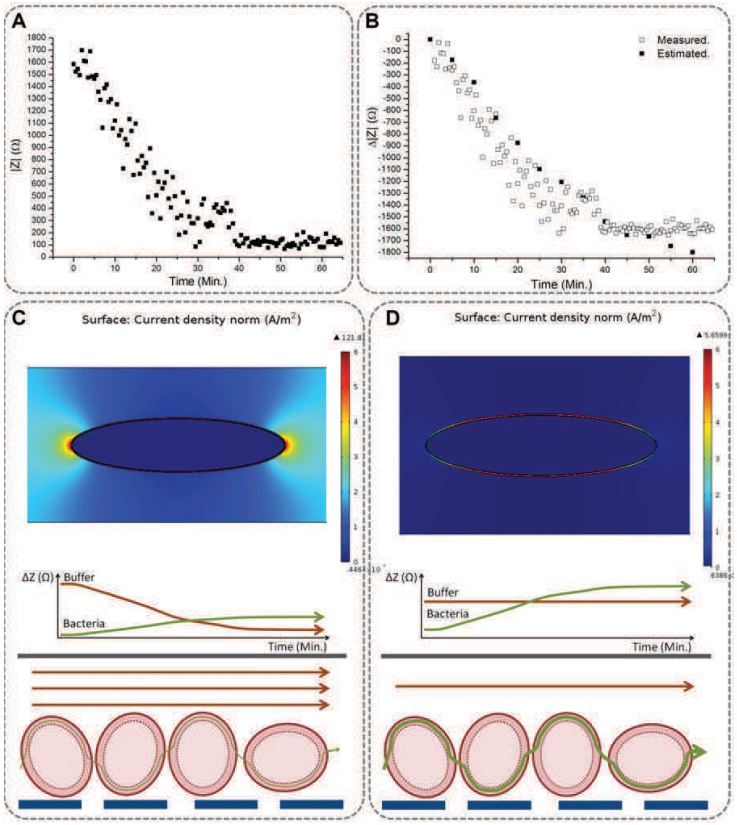

Figure 5. (A) Impedance magnitude measured during the trapping operation. (B) Experimental versus estimated impedance magnitude relative incremental changes. (C) Comsol multiphysics simulation of a single diluted cell on high-conductivity buffer (0.5×10^{-3}–2.5×10^{-3} S/m). Schematic modelization of current flow path and contribution to impedance measurement of both buffer and trapped bacteria. (D) Comsol multiphysics simulation of a single diluted cell on low-conductivity steady buffer (Milli-Q water, 8.2×10^{-5} S/m). Schematic modelization of current flow path and contribution to impedance measurement of both buffer conductivity and trapped bacteria.

of the device working protocol assuring a reliable impedance measurement.

In the resulting protocol, the microfluidic chip was first filled with Milli-Q water media to obtain the threshold impedance measurement. Afterward, a 50 μL sample of *E. coli* was injected through a controlled valve to the microfluidic chip and trapped by DEP forces while flowing continuously at 10 μL/min, higher flow rate compared with other solutions for DEP and IA combination, such as 2–4 μL/min [30]. After each 50 μL sample of bacteria was injected into the channel, 50 μL of Milli-Q water, with a specified conductivity of 8.2×10^{-5} S/m, was automatically injected at 10 μL/min to ensure a steady media conductivity for the impedance measurement. Once the Milli-Q water was injected, the impedance electronic module was activated and the DEP generator deactivated by means of multiplexor. Four contiguous impedance measurements were performed each time in order to evaluate precision. Afterward, another 50 μL sample of *E. coli* was injected and the process repeated until all the samples were injected. So, the impedance measurement is always performed after each 50 μL bacteria sample was injected, trapped, and cleaned. The whole process was performed to scan the 500 Hz to 5 kHz IA frequency range each 100 Hz. The DEP was generated by applying two 15 Vpp counter-phased signals through the IDEs. The results of the experimental impedance measurements for three frequencies (500, 1700, and 5000 Hz) are depicted in Fig. 6.

Results are depicted as the increment ($\Delta|Z| = |Z| - |Z_0|$) between the different impedance magnitude measurements for every bacteria sample injected ($|Z|$) and the initial media impedance magnitude measurement ($|Z_0|$). Figure 6A depicts $\Delta|Z|$ measurements through time for the initial and final frequency value, 500 Hz and 5 kHz, respectively, as well as the 1.7 kHz frequency $\Delta|Z|$ measurements, which seem to be more sensitive and reliable with an accuracy error of less than 2% of bacteria concentration with a correlation of 0.988. Precision can be evaluated with the coefficient of variation, which is the SD of the four experiment repetitions divided by the mean value of the four repetitions' measurement. The mean value of the coefficient of variation is 3.1% on the whole range, although the device is more precise for lower bacteria concentration levels where the coefficient of variation is below 3%.

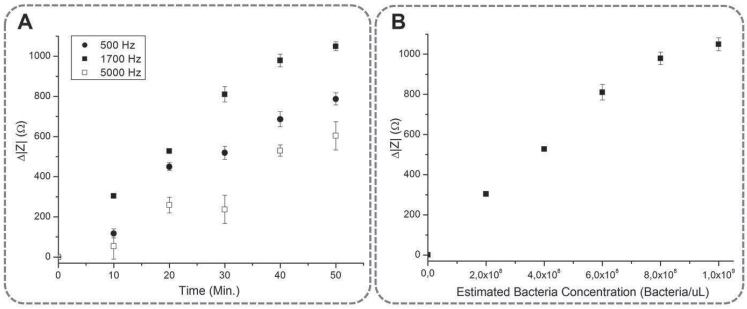

Figure 6. (A) Impedance magnitude measured changes during bacterial sample on-chip concentration at several given times. Medium cleaning procedure was performed before each measurement. (B) Impedance magnitude measurements at 1700 Hz related to estimated bacteria concentrations.

Thus, steady and sensitive $\Delta|Z|$ measurement at different frequencies, which is bacteria dependent, was observed. Furthermore, bioimpedance control of the achieved sample concentration showed a reliable sensitivity for the protocol including a bacteria-cleaning step. The controlled and steady low media conductivity microenvironment solves issues regarding overall system viability.

The DEP module had a proven trapping efficiency of $85.65 \pm 1.07\%$, for a single 50 μL bacteria sample injected at continuous flow of 10 μL/min, by measuring the escaped and the collected bacteria of a single load by cytometric analysis [40]. Although the whole process trapping efficiency had not been tested, each sample load was estimated to increment the bacteria concentration 2×10^8 bacteria/mL inside the microfluidic chip. Figure 6B depicts the $\Delta|Z|$ measurements for each bacteria concentration increment (bacteria/μL) when 1.7 kHz frequency is applied. However, our main goal was to verify that the process of bacterial concentration while monitoring the concentration is feasible, as it has been proved. The measured impedance values were related to the quantity of bacteria concentrated with a correlation of 0.988 and a coefficient of variation of 3.1%, avoiding distortion and instability related to undesired effects such as media conductivity variations and DEP voltage interferences.

5 Concluding remarks

Here we describe a novel device and automated protocol, based on DEP and IA, to concentrate bacteria in benchtop setups in a controlled manner. The system consists of a microfluidic chip, with integrated electrodes, and its associated custom instrumentation electronics. It performs bacteria injection, trapping, cleaning, and continuous short-time impedance measuring while achieving the desired levels of concentration. As a proof of concept, it has been applied to concentrate *E. coli* and to automatically monitor its concentration. The electronic apparatus was validated using a microfluidic chip with four integrated gold electrodes specifically designed for the application. The automated system was tested by trapping and measuring samples of *E. coli* 5K at a concentration of 2×10^7 cells/mL. Concentration and real-time detection of the trapped bacteria inside the microfluidic chip were proven, working a high flow injection rate, up to 10 μL/min, for different buffer conductivities [31, 32]. Bacteria media conductivity, and its variability, was demonstrated to be a challenging issue when monitoring concentration by means of IA. An automated protocol integrated in the overall system was proposed to solve this problem, strengthening the system versatility and robustness. Before each measurement, the designed system cleans the bacteria samples periodically, while trapped on the microfluidic chip, with Milli-Q water at a controlled conductivity of 8.2×10^{-5} S/m. To our best knowledge, this proposed system is a useful tool to solve some current microbiology laboratories shortcomings. Bacteria can be concentrated to given specifications while performing analytical procedures. The development of LoC-based equipment, removing the need of huge and expensive devices, is an important research field aiming for smaller systems with better functionalities, such as the integrated application specific integrated system stimulator for electrokinetically driven microfluidic devices presented by Gomez-Quiñones et al. [52]. Nowadays, electronic technology allows further miniaturization of devices such as our concentrator. A SOI technology such as XTO18 from XFAB would be suitable to combine digital instrumentation and class E amplifiers inside a unique chip. However, some drawbacks must be considered when integrating the full system into the LoC device, as it would either increase disposable cost or reduce applicability due to possible contaminations. Still, the simplicity of the presented microfluidic device and the development of the custom electronics on a single application specific integrated system, along with an automated procedure protocol, pushes toward the development of robust and reliable LoC automated bacterial concentrator relying on DEP concentration and IA monitoring.

This work was financially supported by the THERAEDGE project (FP7-ICT-2007-216027), funded by the "Information and Communication Technologies" programme under the 7th Research Framework Programme of the European Union. The Nanobioengineering group is supported by the Commission for Universities and Research of the Department of Innovation, Universities, and Enterprise of the Generalitat de Catalunya (2009 SGR 505). This work was supported by Obra Social "La Caixa." CIBER-BBN is an initiative funded by the VI National R&D&i

Plan 2008–2011, Iniciativa Ingenio 2010, Consolider Program, CIBER Actions, and financed by the Instituto de Salud Carlos III with assistance from the European Regional Development Fund. This material is based upon work supported by the Botín Foundation, Santander, Spain.

The authors have declared no conflict of interest.

6 References

[1] Pethig, R., *Biomicrofluidics* 2010, *4*, 22811.

[2] Sun, T., Morgan, H., *Microfluid. Nanofluidics* 2010, *8*, 423–443.

[3] Hamada, R., Takayama, H., Shonishi, Y., Mao, L., Nakano, M., Suehiro, J., *Sens. Actuators B Chem.* 2013, *181*, 439–445.

[4] Agarwal, S., Sebastian, A., Forrester, L. M., Markx, G. H., *Biomicrofluidics* 2012, *6*, 24101–2410111.

[5] Fatoyinbo, H. O., Hoettges, K. F., Hughes, M. P., *Electrophoresis* 2008, *29*, 3–10.

[6] Venkatanarayanan, A., Keyes, T. E., Forster, R. J., *Anal. Chem.* 2013, *85*, 2216–2222.

[7] Xu, M., Luo, X., Davis, J. J., *Biosens. Bioelectron.* 2013, *39*, 21–25.

[8] Feldsine, P. T., Falbo-Nelson, M. T., Hustead, D. L., *J. AOAC Int.* 1994, *77*, 58–63.

[9] Pouch Downes, F., Ito, K., *Compendium of Methods for the Microbiological Examination of Foods*, 4th edition, American Public Health Association, Washington, DC, USA. 2001, p. 676.

[10] Morgan, H., Green, N. G., *AC Electrokinetics: Colloids and Nanoparticles*, Research Studies Press, Philadelphia, PA, USA. 2003.

[11] Pohl, H. A., *J. Appl. Phys.* 1951, *22*, 869.

[12] Chin, C. D., Linder, V., Sia, S. K., *Lab Chip* 2007, *7*, 41–57.

[13] Figeys, D., Pinto, D., *Anal. Chem.* 2000, *72*, 330 A–335 A.

[14] Stone, H. A., Stroock, A. D., Ajdari, A., *Annu. Mech.* 2004, *36*, 381–411.

[15] Lapizco-Encinas, B. H., Simmons, B. A., Cummings, E. B., Fintschenko, Y., *Anal. Chem.* 2004, *76*, 1571–1579.

[16] Braff, W. A., Pignier, A., Buie, C. R., *Lab Chip* 2012, *12*, 1327–1331.

[17] Gascoyne, P. R. C., Noshari, J., Anderson, T. J., Becker, F. F., *Electrophoresis* 2009, *30*, 1388–1398.

[18] Gascoyne, P., Mahidol, C., Ruchirawat, M., Satayavivad, J., Watcharasit, P., Becker, F. F., *Lab Chip* 2002, *2*, 70–75.

[19] Moon, H. S., Kwon, K., Kim, S. I., Han, H., Sohn, J., Lee, S., Jung, H. I., *Lab Chip* 2011, *11*, 1118–1125.

[20] Fatoyinbo, H. O., McDonnell, M. C., Hughes, M. P., *Biomicrofluidics* 2014, *8*, 044115.

[21] Zordan, M. D., Grafton, M. M. G., Acharya, G., Reece, L. M., Cooper, C. L., Aronson, A. I., Park, K., Leary, J. F., *Cytometry A* 2009, *75*, 155–162.

[22] Deisingh, A. K., Thompson, M., *Analyst* 2002, *127*, 567–581.

[23] Hahm, B.-K., Bhunia, A. K., *J. Appl. Microbiol.* 2006, *100*, 1017–1027.

[24] Bohaychuk, V. M., Gensler, G. E., King, R. K., Wu, J. T., McMullen, L. M., *J. Food Protoc.* 2005, *68*, 2637–2647.

[25] Hong, B.-X., Jiang, L.-F., Hu, Y.-S., Fang, D.-Y., Guo, H.-Y., *J. Microbiol. Methods* 2004, *58*, 403–411.

[26] Foudeh, A. M., Fatanat Didar, T., Veres, T., Tabrizian, M., *Lab Chip* 2012, *12*, 3249–3266.

[27] Ramírez, N., Regueiro, A., Arias, O., Contreras, R., Biotecnol. Apl. 2009, *26*, 72–78.

[28] Dweik, M., Stringer, R. C., Dastider, S. G., Wu, Y., Almasri, M., Barizuddin, S., *Talanta* 2012, *94*, 84–89.

[29] Grossi, M., Lanzoni, M., Pompei, a, Lazzarini, R., Matteuzzi, D., Riccò, B., *Biosens. Bioelectron.* 2010, *26*, 983–990.

[30] Dastider, S. G., Barizuddin, S., Dweik, M., Almasri, M., *RSC Adv.* 2013, *3*, 26297–26306.

[31] Park, S., Zhang, Y., Wang, T.-H., Yang, S., *Lab Chip* 2011, *11*, 2893–2900.

[32] Rozitsky, L., Fine, A., Dado, D., Nussbaum-Ben-Shaul, S., Levenberg, S., Yossifon, G., *Biomed. Microdevices* 2013, *15*, 859–865.

[33] Croxen, M. A., Law, R. J., Scholz, R., Keeney, K. M., Wlodarska, M., Finlay, B. B., *Clin. Microbiol. Rev.* 2013, *26*, 822–880.

[34] Sievert, D. M., Ricks, P., Edwards, J. R., Schneider, A., Patel, J., Srinivasan, A., Kallen, A., Limbago, B., Fridkin, S., *Infect. Control Hosp. Epidemiol.* 2013, *34*, 1–14.

[35] Ulett, G. C., Totsika, M., Schaale, K., Carey, A. J., Sweet, M. J., Schembri, M. A., *Curr. Opin. Microbiol.* 2013, *16*, 100–107.

[36] Dhama, K., Chakraborty, S., Tiwari, R., Verma, A. K., Saminathan, M., Amarpal, Y. S. M., Nikousefat, Z., Javdani, M., Khan, R. U, Res. Opin. Anim. Vet. Sci., *3*, 179–194.

[37] Sabounchi, P., Morales, A. M., Ponce, P., Lee, L. P., Simmons, B. A., Davalos, R. V, *Biomed. Microdevices* 2008, *10*, 661–670.

[38] Jones, T. B., *Electromechanics of Particles*, Cambridge University Press, 2005, Cambridge, UK.

[39] Castellarnau, M., Errachid, A., Madrid, C., Juárez, A., Samitier, J., *Biophys. J.* 2006, *91*, 3937–3945.

[40] Moral Zamora, B. del, *Micro Nanosyst.* 2014, *6*, 856–859.

[41] Fairooz, T., Istya, S., *Int. J. Biol. Life Sci.* 2011, *5*, 912–924.

[42] Patterson, R., in: Bronzino, J. D. (Ed.), *Biomedical Engineering Handbook*, 2000, CRC Press, Boca Raton, 734–773.

[43] Martinson, O. G., Grimnes, S., *Bioimpedance and Bioelectricity Basics,* 2008, Academic Press, Waltham, MA, USA.

[44] Lenaerts, B., Puers, R., *Omnidirectional Inductive Powering for Biomedical Implants*, Springer, Dordrecht, Netherlands, 2009.

[45] Rasid, M. H., González, M. H. R. V., Fernández, P. A. S., *Electrónica de potencia: Circuitos, dispositivos y aplicaciones*, Pearson Educación, New York, NY, USA, 2004.

[46] Sokal, N. O., *QEX Commun. Quart.* 2001, *204*, 9–20.

[47] Cheng, M. S., Ho, J. S., Lau, S. H., Chow, V. T. K., Toh, C.-S., *Biosens. Bioelectron.* 2013, *47*, 340–344.

[48] Yang, L., *Talanta* 2008, *74,* 1621–1629.

[49] Punter-Villagrasa, J., Colomer-Farrarons, J., Miribel, P. L., Rinken, T. (Ed.), *Bioelectronics for Amperometric Biosensors*, Intech 2013. Available at: http://www.intechopen.com/books/state-of-the-art-in-biosensors-general-aspects/bioelectronics-for-amperometric-biosensors.

[50] Varshney, M., Li, Y., *Biosens. Bioelectron.* 2009, *24,* 2951–2960.

[51] Li, M., Li, S., Cao, W., Li, W., Wen, W., Alici, G., *Microfluid. Nanofluidics* 2013, *14,* 527–539.

[52] Gomez-Quiñones, J., Moncada-Hernández, H., Rossetto, O., Martinez-Duarte, R., Lapizco-Encinas, B.H., Madou, M., Martinez-Chapa, S.O. *New Circuits and Systems Conference (NEWCAS)* 2011, 350–353.

